Running head: Penetration depth and sediment resuspension by bottom trawls

Comparison of mechanical disturbance in soft sediments due to tickler-chain SumWing trawl versus electro-fitted PulseWing trawl

Jochen Depestele[1*], Koen Degrendele[2], Moosa Esmaeili[3], Ana Ivanović[3], Silke Kröger[4], Finbarr G. O'Neill[5], Ruth Parker[4], Hans Polet[1], Marc Roche[2], Lorna R. Teal[6], Bart Vanelslander[1], Adriaan D. Rijnsdorp[6]

[1] *Flanders Research Institute for Agriculture, Fisheries and Food (ILVO), Fisheries research group, Ankerstraat 1, 8400 Oostende, Belgium*

[2] *Federal Public Service Economy, Energy – Continental Shelf, North Gate 4B26, Koning Albert II-laan 16, B-1000 Brussels, Belgium*

[3] *School of Engineering, Fraser Noble Building, University of Aberdeen, Aberdeen, AB24 3UE, UK*

[4] *Centre for Environment, Fisheries and Aquaculture Science (Cefas), Lowestoft Laboratory, Pakefield Road, Lowestoft, Suffolk NR33 0HT, UK*

[5] *Technical University of Denmark, National Institute of Aquatic Resources (DTU – AQUA), Willemoesvej 2, 9850 Hirtshals, Denmark*

[6] *Wageningen Marine Research, Wageningen UR, PO Box 68, 1970 AB, IJmuiden, the Netherlands*

*E-mail of corresponding author: jochen.depestele@ilvo.vlaanderen.be

Abstract

Ecosystem-based management strategies increasingly require assessments of bottom trawling impacts on benthic habitats at the detailed level of different gear types. Two types of bottom trawls for catching flatfish (tickler-chain SumWing and electrode-fitted PulseWing trawls) were compared by combining several observational and modelling techniques to assess the changes in trawl penetration and associated effects on the seabed texture and sediment sorting. Bathymetrical measurements using a multi-beam echo sounder (MBES) confirmed that the SumWing trawl tracks were consistently and uniformly deepened to 1.5 cm depth in contrast to 0.7 cm following PulseWing trawling. MBES backscatter strength analysis indicated that SumWing trawls (3.11 dB) also flattened seabed roughness significantly more than PulseWing trawls (2.37 dB). Sediment Profile Imagery (SPI) showed that SumWing trawls (mean, standard deviation) homogenised the sediment deeper (3.4 cm, 0.9 cm) and removed more of the oxidised layer than PulseWing trawls (1 cm, 0.8 cm). SPI imagery showed that the reduced PulseWing trawling impacts allowed a faster re-establishment of the oxidised layer and micro-topography in contrast to SumWing trawling. Particle size analysis suggested that SumWing trawls injected finer particles into the deeper sediment layers (~4 cm depth), while PulseWing trawling only caused coarsening of the top layers (winnowing effect). This is in agreement with numerical modelling, which predicted that SumWing trawls would penetrate deeper into the sediment than PulseWing trawls. The total penetration depth (mean, standard deviation) of the SumWing trawls (4.1 cm, 0.9 cm) and PulseWing trawls (1.8 cm, 0.8 cm) was estimated by measuring the depth of the disturbance layer and by modelling the erosion of the surficial sediments due to sediment mobilisation in the wake of the gear (SumWing = 0.7 cm; PulseWing trawl = 0.8 cm). Our study has shown that PulseWing trawls reduced most of the mechanical

trawling impacts on the seabed compared to SumWing trawls for this substrate and area characteristics.

Keywords: beam trawl, biogeochemistry, habitat impacts, particle size distribution, penetration depth, pulse trawl, seafloor integrity, sediment resuspension

1. Introduction

Demersal otter trawls and beam trawls are the most widely used fishing gears to catch bottom dwelling fish, crustaceans and bivalves (FAO, 2016; Cashion et al., 2018) and are the most widespread source of physical disturbance to marine habitats (Oberle et al., 2016; Eigaard et al., 2017; Kroodsma et al., 2018). The development and implementation of ecosystem-based management strategies increasingly require assessments of bottom trawling impacts on the seabed. Risk-based assessments are an appropriate tool for this purpose. These and others are being developed for the implementation of the European Marine Strategy Framework Directive, Descriptor 6 'Sea-floor integrity' (Rijnsdorp et al., 2016; EU, 2017).

The risk of a significant adverse impact on the sea-floor (seabed) depends on (1) the likelihood of exposure and (2) sensitivity of the seabed to fishing activities (Knights et al., 2015). The likelihood of exposure relates to the overlap of distribution of habitat types and fishing effort (Eigaard et al., 2017), while 'sensitivity' depends on the ability to withstand fishing pressure and recover from the damage imposed (Tyler-Walters et al., 2009; Depestele et al., 2014). Quantifying impact is difficult but approaches are emerging that express impact as a function of mortality and the recovery rate (Pitcher et al., 2017). Mortality is defined as the proportion of seabed biota killed by a single trawl pass. Mortality is very difficult to estimate due to the high spatial variability of benthic organisms (Collie et al., 2000; Kaiser et al. 2006; Løkkeborg, 2007; Hiddink et al., 2017; Sciberras et al., 2018). Measuring the trawling penetration depth is likely to be a cost-effective alternative to estimate the direct mortality imposed by bottom trawling, and allows benthic impacts across fishing gears to be compared (Eigaard et al., 2016; Hiddink et al., 2017; Pitcher et al., 2017; Sciberras et al., 2018). These novel insights set the baseline for assessing trawling impact, but require more detail at the level of

different gear types to enable implementation in fisheries management (Kaiser et al., 2016). Different demersal gear types are designed to have different levels of seabed contact or penetration, depending on the target species, their catching stimulus and seabed type. These factors contribute to different penetration depths, but have until now only been assessed for generic gear designs (Eigaard et al., 2016; Sciberras et al., 2018). Different gear configurations and the quantification of their potential benefits for mitigation of seabed impacts, cannot be ignored any longer and were identified as one of the top 10 knowledge priorities for managing seabed impact (Kaiser et al., 2016).

The flatfish-directed trawler fleet in the North Sea has evolved over the last decade and used different gear configurations (Haasnoot et al., 2016). Conventional tickler-chain trawls tow a number of chains over the seabed to chase flatfish out of the seabed (Rijnsdorp et al., 2008). The net is opened horizontally by a steel bar (the beam) supported by two trawl shoes at each end to maintain the beam at a constant height above the seabed and maintain the vertical opening of the net. In pulse trawls, the tickler chains are replaced by electrodes that induce a cramp response that bends the fish into a U-shape, thus allowing them to be scooped up by the ground gear (Soetaert et al., 2015a; de Haan et al., 2016). The pulse trawls are towed at a lower speed, and may catch sole more selectively and reduce discards of benthos (van Marlen et al., 2014). The beam and the two trawl shoes of the conventional tickler-chain trawl and the pulse trawl may be replaced by a wing-shaped foil with a ‘nose’ in the centre. This wing-shaped foil was designed to reduce drag in the water and on the seabed. A tickler-chain trawl using a foil is called a ‘SumWing’ trawl, while a trawl using the foil in combination with electric pulses is called a ‘PulseWing’ trawl. In 2010, 30% of the Dutch flatfish-directed trawler effort was represented by beam trawls using the SumWing with tickler chains, 8% using electric pulses and 62% using the conventional

beam trawl. In 2016, 12% of the effort came from SumWing trawls, 83% came from pulse trawls, while only 5% was exerted by conventional beam trawls (www.agrimate.nl; last accessed: 7 May 2018). In 2016, 19% of the pulse trawls used a steel bar with shoes as opposed to the wing-shaped foil (PulseWing trawl) to open the net.

In this study we examined differences in seabed impacts between two gear configurations used to target flatfish (Dover sole (*Solea solea*) in particular). We compared the mechanical impact on the seabed of a SumWing trawl with a PulseWing trawl, with a particular focus on the comparison of penetration depths. The penetration depth of a trawl is difficult to quantify. The passage of a trawl disturbs the top layer of the sediment, which can (i) remain in the same location, (ii) be compressed or compacted, (iii) be laterally displaced (Gilkinson et al., 1998; Ivanović and O'Neill, 2015) or (iv) be mobilised and carried away from the area to a distance dependent upon the particle size and bottom currents (Depestele et al., 2016; Mengual et al., 2016). Sediment reworking, mobilisation and transport leads to sediment erosion (Pilskaln et al., 1998; Palanques et al., 2001; Durrieu de Madron et al., 2005), altered seabed morphology (Eleftheriou and Roberston, 1992; Schwinghamer et al., 1998; Currie and Parry, 1999) and changes in the lithological and geochemical characteristics of the seabed (Duplisea et al., 2001; Puig et al., 2012; Oberle et al., 2018). We carried out a field experiment using complementary sampling approaches to improve our understanding of the acute changes to the seabed by two commercial trawl types in the North Sea.

123 ## 2. Material and methods

124 ### *2.1 Background to this study*

125 In Depestele et al. (2016) we compared the seabed impact of bottom trawls using tickler
126 chains versus electric pulses to catch flatfish in the North Sea. This study elaborates on
127 the previous findings in 2 main ways. First, Depestele et al. (2016) focussed on one
128 branch of the flatfish-directed trawler fleet, i.e. 'euro-cutter' vessels with engine power
129 below 300 HP (≤221 kW), and access to coastal waters between 3 and 12 nautical
130 miles, including the Plaice Box (Mills et al., 2007; Rijnsdorp et al., 2008; Beare et al.,
131 2013). This study focussed on the other branch, the large trawler fleet with engine
132 power > 300 HP, operating in offshore waters with heavier and larger trawls. The main
133 differences in gear parameters and location characteristics of two fleets are reflected in
134 both case studies (Table S1 in Suppl. Mat.; Lindeboom and de Groot, 1998).
135 The other differences, despite the analogous modelling approaches in both case studies,
136 were experimental design, sampling equipment and studied parameters differed (Table
137 S1 in Suppl. Mat.). Depestele et al. (2016) focused on bathymetrical changes using the
138 multi-beam echo sounding (MBES), but could not directly compare the effects of
139 tickler-chain and pulse trawling due to differences in trawling intensities at the
140 experimental sites. In that study, we measured sediment mobilisation in situ using the
141 LISST-100X, which was not deployed in the present study. In this study we used MBES
142 bathymetry data to directly compare one passage of a SumWing trawl versus a
143 PulseWing trawl. We additionally analysed the MBES backscatter data and collected
144 ground truthing data. Sediment samples were collected using a box corer and were
145 analysed to quantify the changes in sediment sorting. The depth of disturbance and
146 biogeochemical changes to cross sections of the seabed were estimated using Sediment

147 Profile Imaging (SPI) after trawling at the same intensities (Rhoads and Cande, 1971,
148 Teal et al., 2008; 2009).

149 ***2.2 Study area***

150 The study area was located between 29 m and 33 m depth in the south-western part of
151 the Frisian Front (southern North Sea, between 53.5692 – 53.5859° N and 4.2664 –
152 4.2999° E). The Frisian Front is a transitional zone in the southern North Sea, located
153 between the shallow, sandy Southern Bight and the deeper, muddy Oyster Grounds
154 (Figure 1). The seabed in this area consists of fine sand with median grain sizes in the
155 range 154 to 163 μm and silt fractions between 12 and 17% (Bockelmann et al., 2018;
156 see Section 3.4). Fine sediment particles settle in this area because tidal currents drop
157 below the critical water velocity (Creutzberg et al., 1984; Stanev et al., 2009).
158 Deposition consists of particulate matter that is transported through the East Anglian
159 turbidity plume and from locally produced phytodetritus and results in a sediment with
160 elevated concentrations of silt, organic carbon and phytopigments (Amaro et al., 2007).

161 ***2.3 Fishing gear***

162 The impact of a 12m SumWing trawl and of a 12m PulseWing trawl were studied. The
163 SumWing trawls were deployed from the FV 'Helena Elisabeth' (TX 29) and the
164 PulseWing trawls from the FV 'Biem van der Vis' (TX43). Both fishing vessels had a
165 length overall (LOA) of ~40 m and a main engine power of approximately 1500 kW.
166 The vessels deployed a pair of 12 m wide trawls from the outrigger booms which are
167 kept open by a wing-shaped foil with a 'nose' in the centre instead of the conventional
168 cylindrical beam with two trawl shoes (Figure S1 and S2 in Suppl. Mat.). The
169 dimensions of the wing-shaped foils did not differ.

The main differences between the gears were related to the stimuli to catch the fish (tickler chains versus electrodes), the geometry of the net opening of the trawl, the ground gears and the nets used (Figure 2 and Figure S2 in Suppl. Mat.). Both trawls had a cod-end with 80 mm stretched diamond-shaped mesh opening as used in the commercial sole fishery (Bayse et al., 2016; Uhlmann et al., 2016), but the SumWing trawl net used during the experiment was lighter than most trawl nets used in the fleet (M. Drijver, skipper of TX29, pers. comm.). The catching process of the SumWing trawl was based on mechanical disturbance by the tickler chains which are rigged in the V-shaped net opening, perpendicular to the towing direction. The SumWing trawls were towed at speeds of ~ 6 kn with a scope ratio of 3 (ratio of warp length to water depth). The total gear weighted nearly 3.1 t in air or 1.6 t in water (HfK engineering, 2018). Eight tickler chains with a chain link diameter of between 18 and 24 mm and a total length between 18.6 and 26 m were attached to the wing. In addition, 9 tickler chains were attached to the middle part of the ground gear. Their length varied between 6 and 14 m, with a chain link diameter was between 13 and 16 mm. Three shorter tickler chains (4.5 - 5 m) with a diameter of 16 mm were attached to the aft part of the ground gear (Figure 2). The ground gear consisted of a 37 m long chain with rubber discs with a diameter between 18 and 28 cm covering the chain over a 7.8 m centre section. The electrodes of the PulseWing trawl were rigged in a longitudinal direction into the square-shaped mouth opening of the trawl net. The PulseWing trawls were towed at fishing speeds of ~5 kn with a scope ratio of 3 (Figure 2). The total gear weighted 2.8 t in air or 1.4 t in water. A total of 27 electrode modules were attached to the wing-shaped foil and the ground gear. The commercial electrodes (*HFK engineering*) have a diameter of 3.3 cm and produce a 60 Hz pulsed bipolar current at 45–50 V with a 0.36 µ*s* pulse duration (Soetaert et al., 2015a; de Haan et al., 2016). A disc-protected rope (of

195 diameter 8 to 10 cm) is rigged alongside each electrode to withstand the tension from
196 towing the gear over the seabed (hereafter called 'tension relief cords'). The mouth of
197 the PulseWing trawl had a square-shaped opening, resulting from two disc-protected
198 chains that were running parallel to the towing direction at the sides of the mouth
199 opening and from two ground ropes, that are both running perpendicular to the towing
200 direction and rigged just in front of the trawl net mouth opening (Figure 2; Figure S2 in
201 Suppl. Mat.). The tension relief cords were attached to the first rubber disc ground gear
202 (diameter = 12 cm), while the net was attached to the second rubber disc ground gear
203 (diameter = 20 cm) (Figure S2 in Suppl. Mat.).

204 ***2.4 Experimental fishing and experimental sites***

205 Acute fishing disturbance by each trawl type was evaluated in a controlled experimental
206 design. We chose 3 sites of 200 x 2800 m (0.56 km²) each, located 250 m apart (Figure
207 1). The PulseWing trawl was fishing in the northern site and the SumWing trawl in the
208 southern site. No fishing took place in the central site, which was used as a control.
209 Samples were taken from this site to measure the influence of factors other than fishing
210 such as waves and currents (Figure 3). The experimental sites were located on a gentle
211 slope with median grain sizes of 154 μm, 162 μm and 169 μm in the PulseWing, control
212 and SumWing trawl sites, respectively. Most particle sizes (down to 10 cm depth)
213 classified as fine sand (125-250 μm): 59% in the PulseWing site, 63% in the control and
214 70% in the SumWing site, with a respective silt fraction of 17%, 13% and 12%. The
215 fine sand fraction in the top layers was similar to the deeper layers, with a slight
216 decrease (5%) in the SumWing site. The mean silt fraction was lower in the top layers
217 than in the deeper layers but its relationship with depth differed between sites.

Six hauls of varying haul duration took place on 10 June 2014 (PulseWing trawl between 8:50-15:00; SumWing trawl between 9:26-14:24). Fishing operations were carried out as similarly as possible, resulting in 13 passages along the length of each site that represented an equal swept area of 0.872 km² and a fishing intensity of 156% (= 0.872 / 0.56 km²) for each gear in their respective experimental site. Observations from the Research Vessel (RV) during the entire experimental period (9-12 June 2014) ensured that no fishing had taken place in the experimental sites other than experimental trawling. Previous trawling disturbances in the experimental sites were limited, as evaluated from prior inspection using multi-beam echo sounding. Historic disturbance by bottom-contacting gears in the area was also low, varying between once every 10 years to once every 2 years (Figure S3 in Suppl. Mat.; Eigaard et al., 2016; 2017).

2.5 Data collection methods

The effects on the seabed were measured using 3 observation techniques: (i) multi-beam echo sounding (MBES) for assessing changes in the sedimentary interface using both bathymetrical and backscatter strength data, (ii) Sediment Profile Imagery (SPI) for identifying geochemical changes and (iii) box corer sampling for particle size analysis. These measurements were collected in all experimental sites before and after fishing during mild weather conditions (significant wave heights < 75 cm; wind speeds < 10 m/s) (see Figure 3 for details).

2.6 Multi-beam echo sounding

Acoustic measurements were performed with the Kongsberg EM2040 single head multi-beam echo sounder (MBES) mounted on the RV Simon Stevin (Depestele et al., 2016). The experimental sites were surveyed before any experimental fishing disturbance began (T0). MBES recordings were obtained by following the fishing vessel at a close distance (< 300 m) during its first trawling passage to estimate changes in seabed bathymetry immediately after fishing (T1; < 0.5 h after fishing). Additional MBES surveys were conducted within 12 h (T2), after 1 day (T3) and after 2 days (T4) (Table 1). All monitoring occurred with a MBES frequency of 320 kHz. Survey lines started and ended 30 to 50 m outside the experimental sites and were conducted at a speed of 8 kn and orientated parallel to the longest side of the sites with an approximate overlap of 30%. MBES measurements across all entire experimental sites were used to assess changes in backscatter strength (BS). BS is used as a proxy to characterise the seabed: higher BS values represent coarse, rough interface with many scatterers (e.g. hard-bodied organisms) while lower BS values represent softer sediment with reduced roughness and fewer scatterers (Ferrini and Flood, 2006).

2.6.1 Seabed bathymetry

A high resolution (0.5 by 0.5 m) digital elevation model of the seabed was created for the MBES survey lines at T0 and T1 by filling an empty grid with validated soundings from the nearest ping in SonarScope (Ifremer, 2016). Trawl tracks were visually detected in the GIS (ArcGIS) on the 0.5 x 0.5 m BS mosaic (Section below). The bathymetrical changes due to fishing were assessed from water depth measurements inside and outside the trawl track. Measurements were selected from equally-spaced (20 m) cross-sections (N = 82 for PulseWing trawl; N = 120 for SumWing trawl) with a mean of > 25 measurements inside the track and > 40 outside the track. The bathymetric

262 profile of each cross-section was corrected for its slope using ordinary least squares
263 regression. The slope-corrected depth measurements inside and outside the track were
264 then compared with a non-parametric Friedman rank sum test following a single factor
265 (water depth) within subject (cross-section) design (Depestele et al., 2016). Statistical
266 differences between water depths inside and outside the trawl tracks were tested for the
267 SumWing and PulseWing trawl at T0 and T1. The deepening of the trawl track was then
268 assessed by subtracting the cumulative depth distribution after fishing from the
269 cumulative depth distribution before fishing. In other words, we first tested whether
270 trawling was conducted on a 'flat' surface, i.e. the locations to be trawled were not
271 positioned shallower or deeper than their surroundings. We then assumed that any
272 differences in water depths found in the trawl track locations at T1 were due to the
273 passage of the trawl.

274 *2.6.2 Seabed backscatter strength*

275 A BS mosaic of 0.5 by 0.5 m resolution was computed for each MBES line. An angular
276 compensation was applied using the mean BS level - incident angle curves computed
277 independently for each line. Only BS values derived from oblique incident angle, inside
278 the angular interval of 30° to 50°, have been considered. The resulting BS mosaics (by
279 line compensated) were merged by experimental site (PulseWing trawl, control and
280 SumWing trawl) and time interval (T0, T2, T3 and T4). BS values from these mosaics
281 were randomly sampled without replacement to increase computational efficiency in
282 further analysis and eliminated as outliers (1.3% of the data) when outside 1.5 times the
283 interquartile (25%-75%) range (1.3% of the data) (Hoaglin and Iglewicz, 1987). This
284 procedure yielded a dataset of > 1700 backscatter values per site and time interval. A
285 linear model was applied to the backscatter values with site, time interval and their
286 interaction as fixed effects. Visual inspection of the histogram and QQ-plot indicated

normality of the residuals and a plot of the residuals versus fitted values confirmed homogeneity of the variances, which allowed ANOVA type III analysis of the model. Significant factors ($P < 0.05$) were tested in *post-hoc* pairwise comparisons with least-square means and p-values were corrected by Tukey-Kramer adjustment for multiple comparisons.

2.7 Sediment Profile Imaging

An SPI camera (sediment profile imagery, Ocean Imaging Systems, North Falmouth, MA, USA) was deployed at each experimental site at four points in time: T0, T1, T2 and T3 (Figure 3). Two replicate images of the sediment were collected at 10 locations per site (Figure 1) (for general principles, see Rhoads and Cande 1971; Germano et al., 2011). The imaging module was based around a Nikon D100 camera (2000 × 3000 pixels = 6 mega pixels, effective resolution = 75 μm × 75 μm per pixel), set to an exposure of 1/60 and a film speed equivalent to ISO 400. These *in situ* images (15 cm × 21.5 cm = 322.50 cm^2) show the apparent redox potential discontinuity (aRPD), which is a reliable proxy for the biological mixing depth (BMD) (Teal et al., 2009; Statham et al., 2018). The depth of this brownish, oxidised layer indicates when biogeochemical redox conditions allow the maximum extent of the presence of particulate iron oxide. The depth of this oxidised layer was quantified using a custom-made, semi-automated macro (modified from Solan et al., 2004) within ImageJ (vs 1.38), a Java-based public domain program developed at the USA National Institutes of Health (available at http://rsb.info.nih.gov/ij/index.html, last accessed 08 February 2018). The depth of the disturbance layer was eliminated when quantifying the oxidised layer post trawling. The effects of trawling and short-time recovery time on the depth of the oxidised layer was assessed using a one-way analysis of variance (ANOVA) with time steps as sources of

311 variation for SumWing and PulseWing trawling separately. Significance of the
312 differences between time steps were tested using a *post-hoc* Tukey's comparison test.
313 The trawling effect at T1 was further assessed using 2 additional parameters. First,
314 surface boundary roughness (i.e. maximum minus minimum depth of penetration) was
315 compared between sites using a one-way ANOVA (Solan et al., 2002) using a *post-hoc*
316 Tukey's comparison test to evaluate differences between sites. Second, the depth of the
317 disturbance layer was analysed using a combination of visual assessment and
318 confirmation within an expert user group. Disturbance layer depths were measured
319 directly on hard-copy after image annotation. The potential influence of the
320 measurements by individual experts (n=3) and the effect of trawl type (SumWing versus
321 PulseWing trawl) on the depth of disturbance were analysed in a linear model with site,
322 time interval and their interaction as fixed effects. Homogeneity of the variances was
323 visually inspected as were the residuals (histogram and QQ plot). A two-way ANOVA
324 type III analysis of the model was conducted using *post-hoc* Tukey's comparisons to
325 assess differences between significant factors. The results were analysed using R 3.3.2
326 for Windows (R Foundation for Statistical Computing, Vienna, Austria).

327 ***2.8 Box corer sampling and particle size distributions***

328 Sediment samples were taken in each experimental site at T0 and T1 (Figure 1; Figure
329 3) using a cylindrical box corer with a diameter of 50 cm and a height of 55 cm,
330 equipped with a valve to prevent flushing or loss of the top layer (de Jong et al., 2015).
331 After recovery of the box corer samples the overlying water was siphoned off, and the
332 sediment surface was carefully studied. In case of disturbance the sample was discarded
333 and a new sample was taken. Small sub cores of 5 cm diameter were taken out of the
334 box corers and sliced in layers of 5 mm (from 0 to 1 cm) and 10 mm (from 1 to 10 cm).
335 Sediment samples were stored in the dark and frozen at -20°C until particle size

336 analysis. Particle size distribution was measured using a Malvern Mastersizer 2000®
337 laser diffractometer using a Hydro 2000G wet sampling system (Malvern, UK). Main
338 parameters applied within the Standard Operating Procedure were a material refractive
339 index of 1.55, a dispersant refractive index of 1.33, stirrer speed at 1000 rpm, pump
340 speed at 2500 rpm, 60s of ultrasonic vibrations during 60s of premeasurement, 15s
341 background time and 15s measurement time.
342 Particle size histograms were plotted before (T0) and after fishing (T1) for each
343 experimental site using a LOESS smoother (span = 0.3) in ggplot2 for R (Wickam,
344 2009). The histograms were drawn for 2 depth categories: 0-1 cm and 1-4 cm. The
345 depth categories were based on differences in mean depth of disturbance of
346 experimental SumWing and PulseWing trawling using SPI results (see Section
347 '*Oxidised layer and depth of disturbance*').
348 The shape of the particle size distributions were largely determined by the silt fraction
349 (<63 μm; 9-15%) and the fine sand fraction (125-250 μm; 50-80%). Both of these
350 fractions were examined in detail as a function of depth, time in relation to fishing (T0
351 and T1) and experimental site. The mean and standard deviation of the silt or fine sand
352 fraction were modelled using Generalized Additive Models (GAM) with a Gaussian
353 error distribution (Wood, 2011). Homoscedasticity and normality assumptions were
354 evaluated through visual examination of plotted standardised residuals versus fitted
355 values and QQ-plots of the residuals. Models with a lower AIC were selected if the
356 ΔAIC was >2. The relationship with depth was first evaluated between experimental
357 sites before fishing (T0) and between experimental sites without fishing disturbance (T0
358 of each site and T1 of the control site). The different relationships of the silt fraction
359 with depth for each experimental site and time step were then compared with the
360 experimental sites after trawling (T1).

2.9 Numerical modelling of penetration depth

Three-dimensional numerical modelling based on the finite element method ABAQUS with Explicit solution was used to simulate interaction processes between the trawls and the seabed (Esmaeili and Ivanović, 2014; 2015). The trawl-seabed interactions were implemented using the Coupled Eulerian Lagrangian (CEL) method with Eulerian mesh based on the volume of fluid method (Dassault, 2014). The flow of the material through the mesh was tracked by computing its Eulerian volume fraction (EVF). The value of EVF represents the portion of material filled; EVF=1 indicates that the element is completely filled with the material and EVF= 0 indicates the element is devoid of the material. The seabed was modelled as elastoplastic, obeying the cap Mohr–Coulomb model criterion, having the following parameters: specific weight of 19.5 kN m^{-3}, Young's modulus of 10 MPa, Poisson's ratio of 0.3, cohesion intercept of 0.01 kPa, angle of internal friction, $\phi = 32°$ and a dilatation angle of 1°. The triaxial test, the shear box test and the one-dimensional compaction test were performed in the laboratory to obtain these parameters. A penalty friction formulation based on Coulomb friction law was used as contact property representing the frictional behaviour between contacting bodies (Esmaeili and Ivanović, 2015). The interaction of the trawls and the seabed was modelled from a reference configuration represented by a cuboid, consisting of two regions: the initial seabed material and a void region. Both regions were discretised using 8-node linear multi-material Eulerian bricks with reduced integration and hourglass control. The trawls were modelled as elastic bodies specified by elastic constants leading to large elastic stiffness. The Lagrangian (trawl) elements were discretised using 4 node quadrilaterals. Their mass and rotary inertia was specified at the centre, and they were given a linear velocity in x-direction, ramping smoothly from zero velocity to a constant value in the next step. In a simulation, the void region was

386 initially empty but filled up with the Lagrangian (trawl) elements and material flowing
387 into the mesh within the Eulerian domain once the passage of a trawl element is
388 simulated. The simulations ran sufficiently long to reach quasi-static condition and were
389 conducted for the nose of the wing-shaped foil of the SumWing and the PulseWing
390 trawl, one single electrode and one single tickler chain with chain link diameter of 24
391 mm.

392 ***2.10 Modelling of sediment mobilisation***

393 The approach of O'Neill and Ivanović (2016) was applied to estimate the quantity of
394 sediment mobilised in the wake of a gear component. Their model estimates the amount
395 of sediment mobilised immediately behind a towed gear component in terms of the
396 hydrodynamic drag of the gear component and the silt fraction of the sediment. It does
397 not predict the fate of the sediment and whether it falls in the track of the component (as
398 is likely for the larger particles) or whether it goes into suspension and is diffused or
399 transported away by ambient currents (as is likely the case for the smaller particle
400 sizes). In Depestele et al. (2016) we applied our model to a 4 m beam trawl and found a
401 good agreement between the model predictions and field measurements.
402 Here we have applied a similar methodology here to measure the amount of sediment
403 mobilised by each of the trawls of our experiments. We calculated the drag of the noses
404 of the wing-shaped foil, the electrodes and the ground gear from experiments on similar
405 shaped objects (Hoerner, 1965; O'Neill and Summerbell, 2016), the drag of the chains
406 from the numerical estimates of Xu and Huang (2014), and the drag of the netting
407 panels in the lower half of the trawl from the empirical model of MacLennan (1981).
408 The silt fraction at each experimental site was estimated from the upper 2 cm sediment
409 layer of the box corer samples taken at T0.

3. Results

3.1 Seabed bathymetry

There was no difference at T0 between the water depths inside and outside the trawl tracks at either site (SumWing trawling location: $\chi^2(df=1)=3.6$, $P = 0.06$; PulseWing trawling location: $\chi^2(df=1)=0.08$, $P = 0.78$). After trawling (T1), the mean (SD) track depths were significantly deeper and were 15.1 (0.9) and 9.1 (1.6) mm for the SumWing and PulseWing trawls, respectively (SumWing trawling location: $\chi^2(df=1)=93.63$, $P < 0.0001$; PulseWing trawling location: $\chi^2(df=1)=17.61$, $P < 0.0001$). The track depth was deeper for the SumWing trawl with a range of depths between 7.6 - 37.5 mm; however the range was wider for the PulseWing trawl (8.9 - 59.5 mm) (Table 2; Figure 4).

3.2 Seabed backscatter strength

Seabed backscatter strength (BS) was statistically different across the experimental sites and time intervals ($F_{6,22031}=126.7$, $P < 0.00001$) (Table S2 in Suppl. Mat.). *Post-hoc* pairwise comparisons indicated that there were no statistical differences between the BS of each experimental site before fishing, but at T2 (after fishing) BS decreased significantly by 9% following SumWing trawling and by 6% following PulseWing trawling (Table 1; Figure 5; Table S3 in Suppl. Mat.). In the adjacent control site, BS was reduced by 1% ($P < 0.05$) from before-fishing conditions (Table 1; Figure 5). After trawling, BS values of the experimentally fished sites increased rapidly in the direction of before-fishing conditions, but this trend attenuated after 1 day (Table 1; Figure 5). The reduction of the BS of the control site persisted over the 2-day observation period.

3.3 Oxidised layer and depth of disturbance

SPI images from T0 conditions show the occurrence of infaunal bioturbators like *Echinocardium* spp. and *Callianassa* spp. and an oxidised/suboxic upper layer of brown particles at both SumWing and PulseWing sites. These observations are consistent with an undisturbed sediment where iron reduction (after use of oxygen, nitrate and manganese) leads to grey colour change of the deeper sediment layers as the brown ferric coatings are lost from particles (Figure 6). The oxidised layer at T1 was intensively disturbed by both the SumWing and the PulseWing trawl. Both trawl types disturbed the upper (oxidised) layers of the sediment and created a homogenised disturbance layer in the upper parts of the sediment profile (Figures 6 & 7). The disturbance layer consisted of both brown particles from the oxidised layer as well as grey/black particles from below and reduced surface boundary roughness significantly following SumWing trawling in comparison to the control site ($F_{2, 58}$=7.74, $P < 0.01$) (Figure 7;Table S4, S5 in Suppl. Mat.). The disturbance layer was sometimes interspersed with mud clasts, particularly in the SumWing images. Reduction of the homogenised layer was greater for the PulseWing trawl (1.0 ± 0.8 cm) and often did not cover the entire SPI image width. The oxidised layer in the SumWing images was either completely removed or a marked boundary was created between the trawling-induced disturbance layer and the relic oxidised layer. The homogenised disturbance layer was more frequent and consistent across the SumWing images and was significantly deeper (3.4 ± 0.9 cm; $F_{1, 114}$=230.555, $P<0.001$) (Figure 8; Table S6, S7 in Suppl. Mat.). The assessment of the disturbance layer did not differ significantly between individual experts ($F_{2, 114}$=2.36, $P = 0.259$) (Table S6 in Suppl. Mat.).

Depending on the trawl penetration, a remnant of the brown oxidised layer sometimes remained visible below this homogenised layer. Over time (1 to 2 days) the brown

456 colour of these particles faded to grey. Also over time the homogenised layer
457 consolidated and the oxic part of the sediment was set up again (within hours of the T2
458 and T3 images) and the redox clines and biological mixing were likely to be re-
459 established. This is shown in the appearance of the iron oxidised surface layers and
460 smoothing of the homogenised layer boundaries in T2 and T3. The oxidised layer in T0
461 was significantly different following SumWing trawling in T1, T2 and T3 ($F_{3, 251}$=33.7,
462 $P < 0.0001$) (Figure 7; Table S8, S9 in Suppl. Mat.). The time required for full recovery
463 following tickler chain trawling exceeded the 48 hour observational period. In contrast,
464 the oxidised layer following PulseWing trawling in T1, T2 and T3, although variable,
465 was not significantly different from T0 ($F_{3, 256}$=2.208, $P = 0.088$) (Figure 7; Table S10,
466 S11 in Suppl. Mat.).

467 ***3.4 Particle size distributions and depth of sediment reworking***

468 The shift in particle size distributions between T0 and T1 in the top layer (0-1 cm)
469 suggested a decrease in smaller particle sizes (silt fraction) and an increase in larger
470 particle sizes (fine sand fraction) in the SumWing and PulseWing sites (Figure 9, upper
471 rows). The T0 and T1 particle size distributions in the control site overlapped and
472 remained largely unchanged in the top 1 cm layer. The particle size distribution in the
473 layer between 1 and 4 cm suggested the same shift in particle size distribution in the
474 control site as in the PulseWing site. The particle size distribution in the SumWing site,
475 in contrast, suggested an opposite trend, which was particularly reflected by the
476 decrease in fine sand fraction after trawling (T0 versus T1 in Figure 9, lower rows).
477 The modelling exercises of 2 primary sediment fractions showed similar patterns of
478 depth of sediment reworking. SumWing and PulseWing trawling decreased the silt
479 fraction in the top layers, but in contrast to PulseWing trawling, the SumWing trawl
480 also caused an increase in the mean silt fraction in the deeper layers (T1 in Figure 10,

upper rows). Similar trends were reflected in the fine sand fraction. Both PulseWing and SumWing trawling increased the fine sand fraction in the top layer, but only SumWing trawling caused a decrease of fine sand in the deeper layers (Figure S4 in Suppl. Mat.). The depth to which both trawling methods affected the seabed was also reflected in the variability of the particle sizes before and after trawling. The variability of the silt and fine sand fraction was low in the control site before and after trawling (Figure 10, and Figure S4 in Suppl. Mat.). The variability in silt and fine sand fractions before fishing was higher in the experimentally fished sites (T0), and was increased by trawling (T1). SumWing trawling increased the variability to a lesser degree (silt fraction: threefold, fine sand fraction: twofold), but its effect also occurred in deeper sediment layers (<4 cm). PulseWing trawling increased the variability in silt fraction (by a factor 3 to 5) and in fine sand fraction (by a factor 2 to 3) but its effect remained limited to the top layers ($\leq$ 2 cm).

3.5 Modelled penetration depth

The seabed deformation following the passage of the nose of a wing-shaped foil is depicted in Figure 11. A number of simulations with different gear weights were conducted to construct a relationship with the average of penetration depths. The penetration depth of the nose varies according to weight following a nearly linear relationship between 1000 and 2000 kg submerged weight (Figure 12). The penetration depths vary between 2.2 and 2.5 cm for the SumWing trawl and between 1.7 and 1.95 cm for the PulseWing trawl. Numerical models were also run for a single electrode and a single tickler chain. Penetration depths varied between 1.5 and 1.9 cm with a mean of 1.7 cm for a single tickler chain while penetration depth of a single electrode varied between 1.0 and 1.5 cm with a mean of 1.2 cm.

3.6 Modelled sediment mobilisation

The amount of silt mobilised is estimated at 10.6 kg.m^2 and 13.1 kg.m^2 for SumWing trawl and PulseWing trawl, respectively. This corresponds to a mobilised sediment layer of 6.6 and 8.2 mm, respectively (assuming a porosity of 0.4). This difference is caused by the different silt fractions of the study sites. The hydrodynamic drag of both gears is very similar although the contribution of the different gear components differs (Table 3). Even though the SumWing trawl is towed at a higher speed (6 kn vs. 5), the hydrodynamic drag of the lower netting panels is less than that of the PulseWing trawl. This is a result of the single twine used in the SumWing trawl and the higher number of panels fitted in the belly section of the PulseWing trawl (Figure S3 in Suppl. Mat.). The hydrodynamic drag of the SumWing gear (ground gear and tickler chains) is greater than that of the PulseWing trawl gear (ground gear and electrodes). The differences between the drag of the 2 types of noses of the wing-shaped foil may be directly attributed to their different towing speeds.

3.7 Total penetration depth

The total penetration depth of the gears is given by the sum of the erosion due to sediment mobilisation (see Section above 'Modelled sediment mobilisation', Table 3) and the mean depth of disturbance (see Section above 'Oxidised layer and depth of disturbance'). Total penetration depth was estimated at 4.1 cm (SD= 0.9 cm) and 1.8 cm (SD= 0.8 cm) for the SumWing and the PulseWing trawl, respectively (Table 4). The variability (SD) in penetration depth is similar (see also penetration profiles in Figure 8), but occurs at different disturbance depths in the seabed.

4. Discussion

Our study has shown that the use of PulseWing trawls instead of SumWing trawls reduced most of the observed mechanical trawling impacts on the seabed for this substrate and area characteristics. The mobilisation of sediment into the water column was comparable between both gears due to lighter trawl nets used in SumWing trawls, but penetration of the seabed by the PulseWing trawl was reduced by more than 50% in comparison to the SumWing trawl. Both trawling types caused tracks and homogenised the seabed topography without full recovery within 48 hours, but seabed impacts of SumWing trawling were consistently higher than those of PulseWing trawling. The SumWing trawl penetrated into the deeper layers (subsurface layer; > 2 cm) and thereby consistently flattened the surface boundary and consistently deepened the seabed along the trawled track. The seabed penetration by the PulseWing trawl varied between skimming off the top mm and penetrating into the subsurface layers, which resulted in a reduced impact on surface boundary roughness and a reduced and highly variable deepening of the seabed. Pulse trawling allowed recovery of the oxidised layer within 48 hours, while this recovery was not observed within 48 hours after SumWing trawling. The lower impact of the pulse trawl is mainly due to the use of electrodes instead of tickler chains. The observed reduction in penetration depth applies to the sediment characteristics of our study area; it may be less in coarser sediments and more in finer sediments. Our results corroborate an earlier study carried out in shallow fine sand habitat in the coastal zone of the southern North Sea (Depestele et al., 2016), where the modelled penetration depths and resultant trawl tracks by euro-cutter vessels were slightly shallower (see Table S1 in Suppl. Mat.). Further work comparing the mechanical, electrical, chemical and biological effects of gears on varying substrates, habitats and hydrographic conditions and associated effects on seabed status and

552 functions will build a more integrated view of gear effects on the seabed overall (ICES,
553 2018).

554 ***4.1 Sediment mobilisation***

555 The sediment mobilisation model predicts that the SumWing trawl mobilised about 1.6
556 mm less sediment into the water column than the pulse trawl. These results were
557 supported by analysis of particle sizes in the top layers of the seabed, where a loss of
558 fine particles was lower following SumWing vs. PulseWing trawling (2.2% in the top 2
559 cm layer after passage of the SumWing as opposed to 2.8% following PulseWing
560 trawling). The limited differences in sediment mobilisation can be attributed to the
561 higher median grain size and lower silt content in the SumWing site than in the
562 PulseWing site and to the use of different netting material and twine thickness. The
563 reduced sediment mobilisation of the SumWing trawl net was compensated by the
564 higher hydrodynamic drag and sediment mobilisation resulting from the ground gear
565 assemblage and the tickler chains. Depestele et al. (2016) found no differences in
566 sediment mobilisation between tickler-chain and PulseWing trawling. While sediment
567 mobilisation was comparable for trawls using tickler chains or pulse electrodes in both
568 case studies, these results should not be directly extrapolated to the tickler-chain or
569 pulse trawler fleet without prior knowledge of gear and operational characteristics of the
570 fleet, such as twine thickness and towing speed.
571 Sediment mobilisation also occurs naturally in the Frisian Front (Amaro et al., 2007). A
572 drop in current velocities below a critical level along the slope of the Frisian Front
573 causes deposition of silt and clay particles and creates a muddy area located to the
574 northeast of the experimental sites (Creutzberg et al., 1984). The tidal ellipses in the
575 Frisian Front area are mostly oriented along a W to E-NE line with a maximum velocity
576 < 50 cm s^{-1} (Van der Molen and de Swart, 2001). Deposition of the finer particles from

neighbouring sites could not be completely ruled out, but was expected to be limited, given the orientation of the tidal ellipses and the experimental sites along the depth contours. Natural movement of sand resulting from tidal or wave currents should not have influenced the deeper sediment layers at the time of the experiment. Aldridge et al (2015: 134) calculated that the seabed in the Frisian Front is not frequently disturbed to a depth of 3 cm per year (1 to 20 times per year). Conversely, sediment in the top layer may have been active. Assuming a depth-mean tidal velocity of < 40 cm/s during the experiment (Davies and Furnes, 1980; Amaro et al., 2007) and using median grain size to calculate seabed roughness resulted in a bed stress of < 0.14 Nm^{-2} (Soulsby, 1997), which is below the critical bed stress for sediment movement (0.16 Nm^{-2}) (Soulsby, 1997:106-109). These calculations use averaged values, which imply that critical bed stress may have been exceeded and may have influenced the top layers. However, the lack of differences in grain size distribution before and after trawling (T0 and T1) suggested that the observed impacts in the top 1 cm layer were due to trawling rather than natural sediment movements (Figure 9). We also expect that the larger sediment particles mobilised by the experimental trawling settled within the experimental sites (200 m wide and ~250 m apart, E-W orientation), given that mean volume concentration of mobilised sediment in the water column drops quickly, e.g. from ~650 µl/l to 80 µl/l at distance of 25 m to 65 m behind the trawl (Fonteyne, 2000; Depestele et al., 2016).

4.2 Seabed topography

The deepening of the trawl tracks altered seabed morphology. Large-scale topographical variation increases with increasing trawling intensities at scales larger than the width of the gear for beam trawls (Depestele et al., 2016). In this study, we show that micro-topographical variation within the trawled tracks decreased. BS analysis suggested a

602 reduced seabed roughness (Ferrini and Flood, 2006) due to the flattening of sand
603 ripples, small pits and mounds, which have also been noted following scallop dredging
604 (Currie and Parry, 1999; Gilkinson et al., 2003; O'Neill et al., 2013) and otter trawling
605 (Eleftheriou and Roberston, 1992; Schwinghamer et al., 1998; Tuck et al; 1998;
606 Mengual et al., 2016).
607 SumWing trawling reduced the seabed roughness the most as tickler chains are towed in
608 perpendicular direction to the towing direction and flatten the seabed across the trawl
609 track (Figure 5). PulseWing trawling reduced BS less as the shallow indentations by the
610 electrodes are caused in parallel direction to the towing direction (Murray et al., 2016).
611 These observations resemble the small depressions caused by rock hopper gear used in
612 otter trawls (Humborstad et al., 2004) or the furrows created by dredges (Dolmer et al.,
613 2001). Visual assessment of underwater footage of electrodes of PulseWing trawls
614 (ILVO, unpublished data) showed that the electrodes do not vibrate or quickly undulate
615 but had a slow lateral motion, and as such flatten seabed features over < 25% of the
616 width of the affected trawl path. Underwater footage also suggested that the tension
617 relief cords (Figure S1 and S2 in Suppl. Mat.) used in PulseWing trawling, are not in
618 direct contact with the seabed. This hypothesis is confirmed by the variation of the
619 bathymetrical changes in Figure 4, i.e. SumWing trawling smoothens the sediment
620 topography more uniformly than PulseWing trawling. BS reduction in the control site
621 was not substantial (< 1 dB) and may reflect the deposition of finer sediment particles
622 on shell fragments or hard-bodied organisms, thereby reducing their potential to act as
623 acoustic scatterers. Small slopes and bed-forms were present in the control site before
624 and after fishing leading to a higher roughness and higher sound scattering (less
625 absorption). These bed-form irregularities were lacking in the PulseWing and SumWing
626 trawling sites following fishing (Figure 5), as was also confirmed by SPI analysis, i.e.

627 the lower surface boundary roughness following trawling (Figure 7). BS analysis
628 showed that the initial smoothening of the trawl tracks (T1) was rapidly counteracted by
629 infaunal activity, i.e. within 24 hours (T2-T4; Figure 5; Table 1) (Briggs and
630 Richardson, 1997). Similarly, the SPI images showed that infaunal activity, along with
631 re-establishment of chemical zonation, contributed to the re-establishment of the
632 oxidised layers (Figure 7) (Smith et al., 2003). BS analysis shows that full re-
633 establishment of the micro-topography was not achieved within 48 hours following
634 either SumWing or PulseWing trawling (Figure 5).

635 ***4.3 Depth of disturbance and sediment reworking***

636 Sediment mobilisation may lead to substantial sediment erosion and deepening of trawl
637 tracks (Dellapenna et al., 2006; Simpsons and Watling, 2006). Depestele et al. (2016)
638 showed that SumWing trawling deepened the track more than would be expected from
639 sediment mobilisation alone. Indeed, our study confirms that the SumWing trawl
640 deepened the track by 13.7 mm, which is more than the 6.6 mm of sediment that the
641 model predicts would be put into the water column due to the hydrodynamic drag. Our
642 study also showed that the deepening of the PulseWing trawl track (7.4 mm) was
643 comparable to 8.2 mm of mobilised sediment predicted by the model. These results
644 suggest that gear components which are designed to interact with the sediment, such as
645 tickler chains which are designed to dig out flatfish from the sediment, cause a more
646 profound effect on the seabed sediment than gear components which are dragged over
647 the seabed surface, such as pulse electrodes. In this study, we examined these
648 geotechnical interactions in more detail by looking at the depth to which particle size
649 distribution and the oxidised layer were affected.
650 Particle size analysis showed that SumWing trawling affected the deeper layers, i.e.
651 down to ~4 cm, whereas PulseWing trawl impacts were limited to the top layers. The

652 depth profile of the silt and fine sand fractions after SumWing trawling (T1) intersected
653 the depth profile before trawling (T0) (Figure 10b). The trend of the depth profile of silt
654 and fine sand fractions after PulseWing trawling was, in contrast to SumWing trawling,
655 not different from untrawled conditions for the deeper layers (1-4 cm). These trends
656 suggest that SumWing trawling mixed fine sediment particles into the deeper layers
657 while PulseWing trawling did not. This vertical mixing by SumWings reduced the
658 vertical gradient in particle sizes, a trend typical of chronically disturbed fishing
659 grounds (Mengual et al., 2016). The deeper seabed impact of the SumWing trawl in
660 particle size analysis was further supported by the SPI analysis, as the presence of mud
661 clasts increased in the SPI images following SumWing trawling (Nilsson and
662 Rosenberg, 2003) and the homogenised layer following SumWing trawling reached
663 deeper than after PulseWing trawl passage.
664 The deeper depth of disturbance and sediment reworking resulted in deeper trawl tracks
665 by the SumWing trawl than the PulseWing trawl. Increased sediment reworking may
666 also have increased sediment compaction into the deeper layers. Sediment compaction
667 implies that the dry bulk density increases after trawling, which may be measured
668 directly (Pusceddu et al., 2014) or suggested indirectly from estimates of seabed
669 'hardness' in RoxAnn surveys (Fonteyne, 2000), from a decreased prism penetration of
670 the SPI (Smith et al., 2003) or from bathymetrical changes (this study). One plausible
671 explanation of increased compaction is suggested by Durrieu de Madron et al. (2005).
672 Pore water is released to the water column from deeper depths in the seabed than the
673 resuspension of fine sediment particles which come only from the top few mm. Deeping
674 of the trawl tracks may be further explained by the disruption of macrofaunal burrows
675 and voids (Smith et al., 2003), particularly when associated with high mortality rates of
676 bioturbators (Gilkinson et al., 2003). The short-term loss of burrows and voids created

by bioturbators is also a likely hypothesis for the deepening of the trawl tracks and sediment compaction in our experiments, given the occurrences of infaunal bioturbators like *Echinocardium* spp. and *Callianassa* spp. in the SPI images and their importance in the Frisian Front (Amaro et al., 2007; Duineveld et al., 2007; Witbaard et al. 2013). The deeper depth of disturbance by the SumWing trawl has likely caused higher mortality rates of infaunal organisms than the PulseWing trawl, since the mortality rate imposed by a bottom trawl is proportional to the penetration depth of the gear (Hiddink et al., 2017; Sciberras et al., 2018). Penetration depth was estimated by combining the measured depth of sediment disturbance and homogenisation from SPI measurements with modelled depth of erosion due to sediment mobilisation. The inferred reduction in mortality rate is related to the effect of mechanical disturbance, primarily due to the replacement of tickler chains. Whether electrical stimulation results in any additional mortality under marine circumstances is yet unknown, but laboratory evidence suggests that exposure to a pulse stimulus will not result in a measurable additional mortality (Soetaert et al. 2015b, 2016; ICES, 2018).

4.4 Implications of the depth of disturbance

Trawling impacts in the top layers caused mobilisation of fine sediment particles which were advected with water currents. This process, known as winnowing, caused a progressive coarsening of surficial sediments and is mirrored in natural processes and stimulated by the activities of extreme bioturbators, which also release fine particles from the top layers and cause an upward coarsening trend (Singer and Anderson, 1984; Briggs and Richardson, 1997; Le Hir et al., 2007; Olsgard et al., 2008; Sciberras et al., 2016). Various studies have demonstrated fine fraction winnowing of intensive long-term bottom trawling and dredging (Caddy et al., 1973; Trimmer et al., 2005; Martín et al., 2014; Mengual et al., 2016; Payo-Payo et al., 2017). Our short-term, acute impact

study confirms these findings by demonstrating the causal link between the loss of fine sediment in the top layers of the fished sites in contrast to the control site (Figure 10). The winnowing effects may increase turbidity (Churchill et al., 1988) and mobilise oxidised sediment particles and nutrients and in due course affect processes in the water column (Dounas et al., 2007; Couceiro et al., 2013).

Whereas both SumWing and PulseWing trawling reworked the top layers of the seabed, SumWing trawling also caused vertical mixing and homogenisation of sediment particles in deeper layers. The replacement of the oxidised layer by a homogenised layer may further retard organic matter cycling by the shift from surficial aerobic to subsurface, anaerobic respiration (Trimmer et al., 2005; Aldridge et al., 2017). This homogenisation does not occur in any natural processes and may have significant ecological implications to the stability of carbon mineralisation and nutrient cycles (Mayer et al., 1991; Duplisea et al., 2001; Sciberras et al., 2016). The deeper depth of disturbance following SumWing trawling also implied that recovery, such as the re-establishment of the oxidised layer, was slower than after disturbance caused by a PulseWing trawl. The inferred higher mortality of bioturbators could have contributed further to the slower recovery following SumWing trawling.

Acknowledgments

This study was part-funded by the EU FP 7 project BENTHIS (grant no. 312088). It does not necessarily reflect the views of the European Commission and does not anticipate the Commission's future policy in this area. We are grateful for the logistic support of VLIZ, the fishermen of TX43 and TX29 and crew members of RV ISIS and RV Simon Stevin during the sea trials and NIOZ for the use of their box corer. ADR and LRT were partly supported by the project "*Impact assessment pulsvisserij*". We are

727 indebted to the skippers and Eddy Buyvoets for drawing the net plans of the trawls. We
728 thank John Aldridge for his insights in sediment transport in relation to natural
729 dynamics; Bavo De Witte for conducting the particle size analysis; Daniel Benden for
730 assisting SPI analyses; Miriam Levenson for English-language editing and Julie
731 Bremner and Stefan Bolam for their critical review. We also wish to thank 3 anonymous
732 reviewers for their constructive comments on earlier drafts of this manuscript.

References

Aldridge, J. N., Parker, E. R., Bricheno, L. M., Green, S. L., and van der Molen, J. 2015. Assessment of the physical disturbance of the northern European Continental shelf seabed by waves and currents. Continental Shelf Research, 108: 121-140.

Aldridge, J. N., Lessin, G., Amoudry, L. O., Hicks, N., Hull, T., Klar, J. K., Kitidis, V., et al. 2017. Comparing benthic biogeochemistry at a sandy and a muddy site in the Celtic Sea using a model and observations. Biogeochemistry, 135: 155-182.

Amaro, T., Duineveld, G., Bergman, M., Witbaard, R., Scheffer, M., 2007. The consequences of changes in abundance of *Callianassa subterranea* and *Amphiura filiformis* on sediment erosion at the Frisian Front (south-eastern North Sea). Hydrobiologia 589: 273-285.

Bayse, S. M., Herrmann, B., Lenoir, H., Depestele, J., Polet, H., Vanderperren, E., and Verschueren, B. 2016. Could a T90 mesh codend improve selectivity in the Belgian beam trawl fishery? Fisheries Research, 174: 201-209.

Beare, D., Rijnsdorp, A. D., Blaesberg, M., Damm, U., Egekvist, J., Fock, H., Kloppmann, M., et al. 2013. Evaluating the effect of fishery closures: Lessons learnt from the Plaice Box. Journal of Sea Research, 84: 49-60.

Bockelmann, F.-D., Puls, W., Kleeberg, U., Müller, D., and Emeis, K.-C. 2018. Mapping mud content and median grain-size of North Sea sediments – A geostatistical approach. Marine Geology, 397: 60-71.

Briggs, K. B., and Richardson, M. D. 1997. Small-scale fluctuations in acoustic and physical properties in surficial carbonate sediments and their relationship to bioturbation. Geo-Marine Letters, 17: 306-315.

Buchanan, J. B. 1966. The biology of *Echinocardium cordatum* [Echinodermata: Spatangoidea] from different habitats. Journal of the Marine Biological Association of the United Kingdom, 46: 97-114.

759 Caddy, J. F. 1973. Underwater observations on tracks of dredges and trawls and some
760 effects of dredging on a scallop ground. Journal of the Fisheries Research Board of
761 Canada, 30: 173-180.

762 Cashion, T., Al-Abdulrazzak, D., Belhabib, D., Derrick, B., Divovich, E., Moutopoulos,
763 D. K., Noël, S.-L., et al. 2018. Reconstructing global marine fishing gear use: Catches
764 and landed values by gear type and sector. Fisheries Research, 206: 57-64.

765 Churchill, J. H., Biscaye, P. E., and Aikman, F. 1988. The character and motion of
766 suspended particulate matter over the shelf edge and upper slope off Cape Cod.
767 Continental Shelf Research, 8: 789-809.

768 Collie, J. S., S. J. Hall, M. J. Kaiser, and I. R. Poiner. 2000. A quantitative analysis of
769 fishing impacts on shelf-sea benthos. Journal of Animal Ecology 69:785-798.

770 Couceiro, F., Fones, G. R., Thompson, C. E. L., Statham, P. J., Sivyer, D. B., Parker,
771 R., Kelly-Gerreyn, B. A., et al. 2013. Impact of resuspension of cohesive sediments at
772 the Oyster Grounds (North Sea) on nutrient exchange across the sediment–water
773 interface. Biogeochemistry, 113: 37-52.

774 Creutzberg, F., Wapernaar, P., Duineveld, G., and Lopez Lopez, N. 1984. Distribution
775 and density of the benthic fauna in the southern North Sea in relation to bottom
776 characteristics and hydrographic conditions. Rapp. P.-v. Réun. Cons. int. Explor. Mer,
777 183: 101-110.

778 Currie, D. R., and Parry, G. D. 1999. Impacts and efficiency of scallop dredging on
779 different soft substrates. Canadian Journal of Fisheries and Aquatic Sciences, 56: 539-
780 550.

781 Dassault, 2014. Dassault Systems, 2014. SIMULA Abaqus Analysis User's Manual
782 Version 6.14.

783 Davies, A. M., and Furnes, G. K. 1980. Observed and Computed M2 Tidal Currents in
784 the North Sea. Journal of Physical Oceanography, 10: 237-257.

785 de Haan, D., J. E. Fosseidengen, P. G. Fjelldal, D. Burggraaf, and A. D. Rijnsdorp.
786 2016. Pulse trawl fishing: characteristics of the electrical stimulation and the effect on

787 behaviour and injuries of Atlantic cod (*Gadus morhua*). ICES Journal of Marine
788 Science 73:1557-1569.

789 de Jong, M. F., Baptist, M. J., Lindeboom, H. J., and Hoekstra, P. 2015. Relationships
790 between macrozoobenthos and habitat characteristics in an intensively used area of the
791 Dutch coastal zone. ICES Journal of Marine Science, 72: 2409-2422.

792 Dellapenna, T. M., Allison, M. A., Gill, G. A., Lehman, R. D., and Warnken, K. W.
793 2006. The impact of shrimp trawling and associated sediment resuspension in mud
794 dominated, shallow estuaries. Estuarine, Coastal and Shelf Science, 69: 519-530.

795 Depestele, J., Courtens, W., Degraer, S., Haelters, J., Hostens, K., Leopold, M., Pinn,
796 E., et al. 2014. Sensitivity assessment as a tool for spatial and temporal gear-based
797 fisheries management. Ocean & Coastal Management, 102, Part A: 149-160.

798 Depestele, J., Ivanović, A., Degrendele, K., Esmaeili, M., Polet, H., Roche, M.,
799 Summerbell, K., Teal, L.R., Vanelslander, B., O'Neill, F.G., 2016. Measuring and
800 assessing the physical impact of beam trawling. ICES Journal of Marine Science 73 (1):
801 i15-i26.

802 Dolmer, P., Kristensen, T., Christiansen, M. L., Petersen, M. F., Kristensen, P. S., and
803 Hoffmann, E. 2001. Short-term impact of blue mussel dredging (*Mytilus edulis* L.) on a
804 benthic community. In Coastal Shellfish — A Sustainable Resource: Proceedings of the
805 Third International Conference on Shellfish Restoration, held in Cork, Ireland, 28
806 September–2 October 1999, pp. 115-127. Ed. by G. Burnell. Springer Netherlands,
807 Dordrecht.

808 Dounas, C., Davies, I., Triantafyllou, G., Koulouri, P., Petihakis, G., Arvanitidis, C.,
809 Sourlatzis, G., et al. 2007. Large-scale impacts of bottom trawling on shelf primary
810 productivity. Continental Shelf Research, 27: 2198-2210.

811 Duineveld, G. C. A., Bergman, M. J. N., and Lavaleye, M. S. S. 2007. Effects of an area
812 closed to fisheries on the composition of the benthic fauna in the southern North Sea.
813 ICES Journal of Marine Science, 64: 899–908.

814 Duplisea, D. E., Jennings, S., Malcolm, S. J., Parker, R., and Sivyer, D. B. 2001.
815 Modelling potential impacts of bottom trawl fisheries on soft sediment biogeochemistry
816 in the North Sea. Geochemical Transactions, 2: 112.

817 Durrieu de Madron, X., Ferré, B., Le Corre, G., Grenz, C., Conan, P., Pujo-Pay, M.,
818 Buscail, R., et al. 2005. Trawling-induced resuspension and dispersal of muddy
819 sediments and dissolved elements in the Gulf of Lion (NW Mediterranean). Continental
820 Shelf Research, 25: 2387-2409.

821 Eigaard, O. R., Bastardie, F., Breen, M., Dinesen, G. E., Hintzen, N. T., Laffargue, P.,
822 Mortensen, L. O., et al. 2016. Estimating seabed pressure from demersal trawls, seines,
823 and dredges based on gear design and dimensions. ICES Journal of Marine Science, 73:
824 i27-i43.

825 Eigaard, O. R., Bastardie, F., Hintzen, N. T., Buhl-Mortensen, L., Buhl-Mortensen, P.,
826 Catarino, R., Dinesen, G. E., et al. 2017. The footprint of bottom trawling in European
827 waters: distribution, intensity, and seabed integrity. ICES Journal of Marine Science,
828 74: 847-865.

829 Eleftheriou, A., and Robertson, M. R. 1992. The effects of experimental scallop
830 dredging on the fauna and physical environment of a shallow sandy community.
831 Netherlands Journal of Sea Research, 30: 289-299.

832 Esmaeili, M., and Ivanović, A. 2014. Numerical modelling of bottom trawling ground
833 gear element on the seabed. Ocean Engineering 91: 316-328.

834 Esmaeili, M., and Ivanović, A. 2015. Analytical and numerical modelling of non-driven
835 disc on friction material. Computers and Geotechnics 68: 208-219.

836 EU 2017. Commission Decision (EU) 2017/848 of 17 May 2017 laying down criteria
837 and methodological standards on good environmental status of marine waters and
838 specifications and standardised methods for monitoring and assessment, and repealing
839 Decision 2010/477/EU. Official Journal of the European Union. L125/43.

840 FAO (2016) The State of World Fisheries and Aquaculture 2018, FAO, Rome.

841 Ferrini V.L., Flood R.D. 2006. The effects of fine-scale surface roughness and grain
842 size on 300 kHz multibeam backscatter intensity in sandy marine sedimentary
843 environments. Marine Geology 228: 153-172.

844 Fonteyne, R. 2000. Physical impact of beam trawls on seabed sediments. In The effects
845 of fishing on non-target species and habitats: biological, conservation and socio-
846 economic issues., pp. 15-36. Ed. by M. J. Kaiser, and S. J. de Groot. Fishing News
847 Books.

848 Germano, J. D., Rhoads, D. C., Valente, R. M., Carey, D. A., and Solan, M. 2011. The
849 use of sediment profile imaging (SPI) for environmental impact assessments and
850 monitoring studies: lessons learned from the past four decades. In Oceanography and
851 Marine Biology: An Annual Review, Vol 49, pp. 235-297. Ed. by R. N. Gibson, R. J. A.
852 Atkinson, and J. D. M. Gordon.

853 Gilkinson, K., Paulin, M., Hurley, S., and Schwinghamer, P. 1998. Impacts of trawl
854 door scouring on infaunal bivalves: Results of a physical trawl door model/dense sand
855 interaction. Journal of Experimental Marine Biology and Ecology, 224: 291–312.

856 Gilkinson, K. D., Fader, G. B. J., Gordon, J., Charron, R., McKeown, D., Roddick, D.,
857 Kenchington, E. L. R., et al. 2003. Immediate and longer-term impacts of hydraulic
858 clam dredging on an offshore sandy seabed: effects on physical habitat and processes of
859 recovery. Continental Shelf Research, 23: 1315-1336.

860 Haasnoot, T., Kraan, M., and Bush, S. R. 2016. Fishing gear transitions: lessons from
861 the Dutch flatfish pulse trawl. ICES Journal of Marine Science, 73: 1235–1243.

862 HfK Engineering. 2018. HfK Engineering website web site [online]. Available at:
863 www.sumwing.nl [Accessed 3 July 18].

864 Hiddink, J., S. Jennings, M. Sciberras, C. Szostek, K. Hughes, N. Ellis, A. D. Rijnsdorp,
865 R. A. McConnaughey, T. Mazor, R. Hilborn, J. Collie, R. Pitcher, R. O. Amoroso, A.
866 Parma, P. Suuronen, and M. Kaiser. 2017. Global analysis of depletion and recovery of
867 seabed biota following bottom trawling disturbance. Proceedings of the National
868 Academy of Sciences 114 (31) : 8301-8306.

869 Hoaglin D.C., Iglewicz B. 1987. Fine-Tuning Some Resistant Rules for Outlier
870 Labeling. Journal of the American Statistical Association 82: 1147-1149.

871 Hoerner, S. F. 1965. Fluid-Dynamic Drag. Hoerner, New Jersey, USA.

872 Humborstad, O.-B., Nøttestad, L., Løkkeborg, S., and Rapp, H. T. 2004. RoxAnn
873 bottom classification system, sidescan sonar and video-sledge: spatial resolution and
874 their use in assessing trawling impacts. ICES Journal of Marine Science 61: 53-63.

875 ICES. 2018. Report of the Working Group on Electric Trawling (WGELECTRA). ICES
876 Report WGELECTRA 2018 17 - 19 April 2018. IJmuiden, the Netherlands. 155pp.

877 Ifremer 2016. http://flotte.ifremer.fr/Presentation-de-la-flotte/Logiciels-
878 embarques/SonarScope (last accessed 23 February 2018).

879 Ivanović, A., and O'Neill, F. G. 2015. Towing cylindrical fishing gear components on
880 cohesive soils. Computers and Geotechnics, 56: 212–219.

881 Kaiser, M. J., K. R. Clarke, H. Hinz, M. C. V. Austen, P. J. Somerfield, and I.
882 Karakassis. 2006. Global analysis of response and recovery of benthic biota to fishing.
883 Marine Ecology-Progress Series 311:1-14.

884 Kaiser, M. J., Hilborn, R., Jennings, S., Amaroso, R., Andersen, M., Balliet, K., Barratt,
885 E., et al. 2016. Prioritization of knowledge-needs to achieve best practices for bottom
886 trawling in relation to seabed habitats. Fish and Fisheries, 17: 637-663.

887 Knights, A. M., Piet, G. J., Jongbloed, R. H., Tamis, J. E., White, L., Akoglu, E.,
888 Boicenco, L., Churilova, T., Kryvenko, O., Fleming-Lehtinen, V., LeppanenJuha-
889 Markku, Galil, B. S., Goodsir, F., Goren, M., Margonski, P., Moncheva, S., Oguz, T.,
890 Papadopoulou, K. N., Setälä, O., Smith, C. J., Stefanova, K., Timofte, F., and Robinson,
891 L. A. 2015. An exposure-effect approach for evaluating ecosystemwide risks from
892 human activities. ICES Journal of Marine Science, 72: 1105–1115.

893 Kroodsma, D. A., Mayorga, J., Hochberg, T., Miller, N. A., Boerder, K., Ferretti, F.,
894 Wilson, A., et al. 2018. Tracking the global footprint of fisheries. Science, 359: 904-
895 908.

Le Hir, P., Monbet, Y., and Orvain, F. 2007. Sediment erodability in sediment transport modelling: Can we account for biota effects? Continental Shelf Research, 27: 1116-1142.

Lindeboom, H. J., and de Groot, S. J. 1998. The effects of different types of fisheries on the North Sea and Irish Sea benthic ecosystems. NIOZ-Rapport 1998-1/RIVO/DLO Report C003/98. 404 pp.

Løkkeborg, S. 2007. Insufficient understanding of benthic impacts of trawling is due to methodological deficiencies. A reply to Gray et al. (2006). Marine Pollution Bulletin, 54: 494-496.

MacLennan, D. N. 1981. The drag of four-panel demersal trawls. Fisheries Research 1: 23-33.

Martín, J., Puig, P., Palanques, A., and Giamportone, A. 2014. Commercial bottom trawling as a driver of sediment dynamics and deep seascape evolution in the Anthropocene. Anthropocene, 7: 1-15.

Mayer, L. M., Schick, D. F., Findlay, R. H., and Rice, D. L. 1991. Effects of commercial dragging on sedimentary organic matter. Marine Environmental Research, 31: 249-261.

Mengual, B., Cayocca, F., Le Hir, P., Draye, R., Laffargue, P., Vincent, B., and Garlan, T. 2016. Influence of bottom trawling on sediment resuspension in the 'Grande-Vasière' area (Bay of Biscay, France). Ocean Dynamics, 66: 1181-1207.

Mills, C. M., Townsend, S. E., Jennings, S., Eastwood, P. D., and Houghton, C. A. 2007. Estimating high resolution trawl fishing effort from satellite-based vessel monitoring system data. ICES J. Mar. Sci., 64: 248-255.

Murray, F., Copland, P., Boulcott, P., Robertson, M., and Bailey, N. 2016. Impacts of electrofishing for razor clams (*Ensis* spp.) on benthic fauna. Fisheries Research, 174: 40-46.

922 Nilsson, H. C., and Rosenberg, R. 2003. Effects on marine sedimentary habitats of
923 experimental trawling analysed by sediment profile imagery. Journal of Experimental
924 Marine Biology and Ecology, 285-286: 453-463.

925 Oberle, F. K. J., Storlazzi C. D. and Hanebuth, T. J. J. 2016. What a drag: Quantifying
926 the global impact of chronic bottom trawling on continental shelf sediment. Journal of
927 Marine Systems 159: 109-119.

928 Oberle, F. K. J., Puig, P., and Martín, J. 2018. Fishing Activities. In Submarine
929 Geomorphology, pp. 503-534. Ed. by A. Micallef, S. Krastel, and A. Savini. Springer
930 International Publishing.

931 Olsgard, F., Schaanning, M. T., Widdicombe, S., Kendall, M. A., and Austen, M. C.
932 2008. Effects of bottom trawling on ecosystem functioning. Journal of Experimental
933 Marine Biology and Ecology, 366: 123-133.

934 O'Neill, F. G., Robertson, M., Summerbell, K., Breen, M., and Robinson, L. A. 2013.
935 The mobilisation of sediment and benthic infauna by scallop dredges. Marine
936 Environmental Research, 90: 104-112.

937 O'Neill F.G. and Summerbell K., 2016. The hydrodynamic drag and the mobilisation of
938 sediment into the water column of towed fishing gear components. Journal of Marine
939 Systems. 164, 76 – 84.

940 O'Neill, F. G., and Ivanović, A. 2016. The physical impact of towed demersal fishing
941 gears on soft sediments. ICES Journal of Marine Science,73: i5-i14.

942 Palanques, A., Guillen, J., and Puig, P. 2001. Impact of bottom trawling on water
943 turbidity and muddy sediment of an unfished continental shelf. Limnology and
944 Oceanography, 46: 1100-1110.

945 Payo-Payo, M., Jacinto, R. S., Lastras, G., Rabineau, M., Puig, P., Martín, J., Canals,
946 M., et al. 2017. Numerical modeling of bottom trawling-induced sediment transport and
947 accumulation in La Fonera submarine canyon, northwestern Mediterranean Sea. Marine
948 Geology, 386: 107-125.

949 Pilskaln, C. H., Churchill, J. H., and Mayer, L. M. 1998. Resuspension of Sediment by
950 Bottom Trawling in the Gulf of Maine and Potential Geochemical Consequences.
951 Conservation Biology, 12: 1223-1229.

952 Pitcher C.R., Ellis N., Jennings S., Hiddink J.G., Mazor T., Kaiser M.J., Kangas M.I.,
953 McConnaughey R.A., Parma A.M., Rijnsdorp A.D., Suuronen P., Collie J.C., Amoroso
954 R., Hughes K.M., Hilborn R. 2017. Estimating the sustainability of towed fishing-gear
955 impacts on seabed habitats: a simple quantitative risk assessment method applicable to
956 data-limited fisheries. Methods in Ecology and Evolution, 8(4), 472-480

957 Puig, P., Canals, M., Company, J., Martin, J., Amblas, D., Lastras, G., Palanques, A., et
958 al. 2012. Ploughing the deep sea floor. Nature, 489: 286-289.

959 Pusceddu, A., Bianchelli, S., Martin, J., Puig, P., Palanques, A., Masque, P., and
960 Danovaro, R. 2014. Chronic and intensive bottom trawling impairs deep-sea
961 biodiversity and ecosystem functioning. Proceedings of the National Academy of
962 Sciences of the United States of America, 111: 8861-8866.

963 Rhoads, D. C., and Cande, S. 1971. Sediment profile camera for in situ study of
964 organisms-sediment relations. Limnology and Oceanography, 16: 110-114.

965 Rijnsdorp, A.D., Poos, J.J., Quirijns, F., HilleRisLambers, R., de Wilde, J.W. , den
966 Heijer, W.M. 2008. The arms race between fishers. Journal of Sea Research 60: 126-
967 138

968 Rijnsdorp A.D., Bastardie F., Bolam S.G., Buhl-Mortensen L., Eigaard O.R., Hamon
969 K.G., Hiddink J.G., Hintzen N.T., Ivanovic A., Kenny A., Laffargue P., Nielsen R.N.,
970 O'Neill F.G., Piet G.J., Polet H., Sala A., Smith C., van Denderen P.D., van Kooten T.,
971 Zengin M.A., 2016. Towards a framework for the quantitative assessment of trawling
972 impacts on the seabed and benthic ecosystem. ICES Journal of Marine Science. 73
973 (suppl 1): i127-i138

974 Schwinghamer, P., Gordon, D. C., Rowell, T. W., Prena, J., McKeown, D. L.,
975 Sonnichsen, G., and Guigné, J. Y. 1998. Effects of experimental otter trawling on
976 surficial sediment properties of a sandy-bottom ecosystem on the Grand Banks of
977 Newfoundland. Conservation Biology, 12: 1215-1222.

978 Sciberras, M., Parker, R., Powell, C., Robertson, C., Kröger, S., Bolam, S., and
979 Hiddink, J. 2016. Impacts of bottom fishing on the sediment infaunal community and
980 biogeochemistry of cohesive and non-cohesive sediments. Limnology and
981 Oceanography, 61(6): 2076–2089.

982 Sciberras, M., Hiddink, J. G., Jennings, S., Szostek, C., Hughes, K. M., Kneafsey, B.,
983 Clarke, L. J., et al. 2018. Response of benthic fauna to experimental bottom fishing: A
984 global meta□analysis. Fish and Fisheries, https://doi.org/10.1111/faf.12283.

985 Simpson, A. W., and Watling, L. 2006. An investigation of the cumulative impacts of
986 shrimp trawling on mud-bottom fishing grounds in the Gulf of Maine: effects on habitat
987 and macrofaunal community structure. ICES Journal of Marine Science, 63: 1616-1630.

988 Singer, J. K., and Anderson, J. B. 1984. Use of total grain-size distributions to define
989 bed erosion and transport for poorly sorted sediment undergoing simulated bioturbation.
990 Marine Geology, 57: 335-359.

991 Smith, C. J., Rumohr, H., Karakassis, I., and Papadopoulou, K. N. 2003. Analysing the
992 impact of bottom trawls on sedimentary seabeds with sediment profile imagery. Journal
993 of Experimental Marine Biology and Ecology, 285-286: 479-496.

994 Soetaert, M., Decostere, A., Polet, H., Verschueren, B., Chiers, K., 2015a.
995 Electrotrawling: a promising alternative fishing technique warranting further
996 exploration. Fish and Fisheries 16: 104-124.

997 Soetaert, M., Chiers, K., Duchateau, L., Polet, H., Verschueren, B., and Decostere, A.
998 2015b. Determining the safety range of electrical pulses for two benthic invertebrates:
999 brown shrimp (*Crangon crangon* L.) and ragworm (*Alitta virens* S.). ICES Journal of
1000 Marine Science, 72: 973-980

1001 Soetaert, M., Verschueren, B., Chiers, K., Duchateau, L., Polet, H., and Decostere, A.
1002 2016. Laboratory study of the impact of repetitive electrical and mechanical stimulation
1003 on brown shrimp *Crangon crangon*. Marine and Coastal Fisheries, 8: 404-411

1004 Solan, M., and Kennedy, R. 2002. Observation and quantification of in situ animal-
1005 sediment relations using time-lapse sediment profile imagery (t-SPI). Marine Ecology
1006 Progress Series, 228: 179-191.

1007 Solan, M., Wigham, B. D., Hudson, I. R., Kennedy, R., Coulon, C. H., Norling, K.,
1008 Nilsson, H. C., et al. 2004. *In situ* quantification of bioturbation using time-lapse
1009 fluorescent sediment profile imaging (f-SPI), luminophore tracers and model
1010 simulation. Marine Ecology Progress Series, 271: 1-12.

1011 Soulsby, R. L. 1997. Dynamics of Marine Sands. Thomas Telford publications, London,
1012 249pp.

1013 Stanev, E. V., Dobrynin, M., Pleskachevsky, A., Grayek, S., and Günther, H. 2009. Bed
1014 shear stress in the southern North Sea as an important driver for suspended sediment
1015 dynamics. Ocean Dynamics, 59: 183-194.

1016 Statham, P. J., Homoky, W. B., Parker, E. R., Klar, J. K., Silburn, B., Poulton, S. W.,
1017 Kröger, S., et al. 2018. Extending the applications of sediment profile imaging to
1018 geochemical interpretations using colour. Continental Shelf Research (in press).
1019 https://doi.org/10.1016/j.csr.2017.12.001.

1020 Teal, L. R., Bulling, M. T., Parker, E. R., and Solan, M. 2008. Global patterns of
1021 bioturbation intensity and mixed depth of marine soft sediments. Aquatic Biology, 2:
1022 207-218.

1023 Teal, L. R., Parker, R., Fones, G., and Solan, M. 2009. Simultaneous determination of in
1024 situ vertical transitions of color, pore-water metals, and visualization of infaunal activity
1025 in marine sediments. Limnology and Oceanography, 54: 1801-1810.

1026 Trimmer, M., Petersen, J., Sivyer, D. B., Mills, C., Young, E., and Parker, E. R. 2005.
1027 Impact of long-term benthic trawl disturbance on sediment sorting and biogeochemistry
1028 in the southern North Sea. Marine Ecology Progress Series, 298: 79-94.

1029 Tuck, I., Hall, S., Roberston, M., Armstrong, E., and Basford, D. 1998. Effects of
1030 physical trawling disturbance in a previously unfished sheltered Scottish sea loch.
1031 Marine Ecology Progress Series, 162: 227-242.

1032 Tyler-Walters, H., Rogers, S. I., Marshall, C. E., and Hiscock, K. 2009. A method to
1033 assess the sensitivity of sedimentary communities to fishing activities. Aquatic
1034 Conservation: Marine and Freshwater Ecosystems, 19: 285-300.

1035 Uhlmann, S.S., Theunynck, R., Ampe, B., Desender, M., Soetaert, M., Depestele, J.,
1036 2016. Injury, reflex impairment, and survival of beam-trawled flatfish. ICES Journal of
1037 Marine Science 73: 1244-1254.

1038 van der Molen, J., and de Swart, H. E. 2001. Holocene tidal conditions and tide-induced
1039 sand transport in the southern North Sea. Journal of Geophysical Research: Oceans,
1040 106: 9339-9362.

1041 van Marlen, B., Wiegerinck, J. A. M., van Os-Koomen, E., van Barneveld, E. 2014.
1042 Catch comparison of pulse trawls and a tickler chain beam trawl. Fisheries Research,
1043 151: 57-69.

1044 Wickham, H. 2009. ggplot2: Elegant Graphics for Data Analysis. Springer-Verlag New
1045 York.

1046 Witbaard, R., Lavaleye, M.S.S., Duineveld, G.C.A. and Bergman, M.J.N. 2013. Atlas of
1047 the megabenthos (incl. small fish) on the Dutch Continental Shelf of the North Sea.
1048 NIOZ-Report 2013-4. 243 pp.

1049 Wood, S. 2011. Package “mgcv”. R package library, version 1.8-15. Available from
1050 http://cran.r-project.org (last accessed 23 February 2018).

1051 Xu, Z., and Huang, S. 2014. Numerical investigation of mooring line damping and the
1052 drag coefficients of studless chain links. Journal of Marine Science and Application, 13:
1053 76-84.

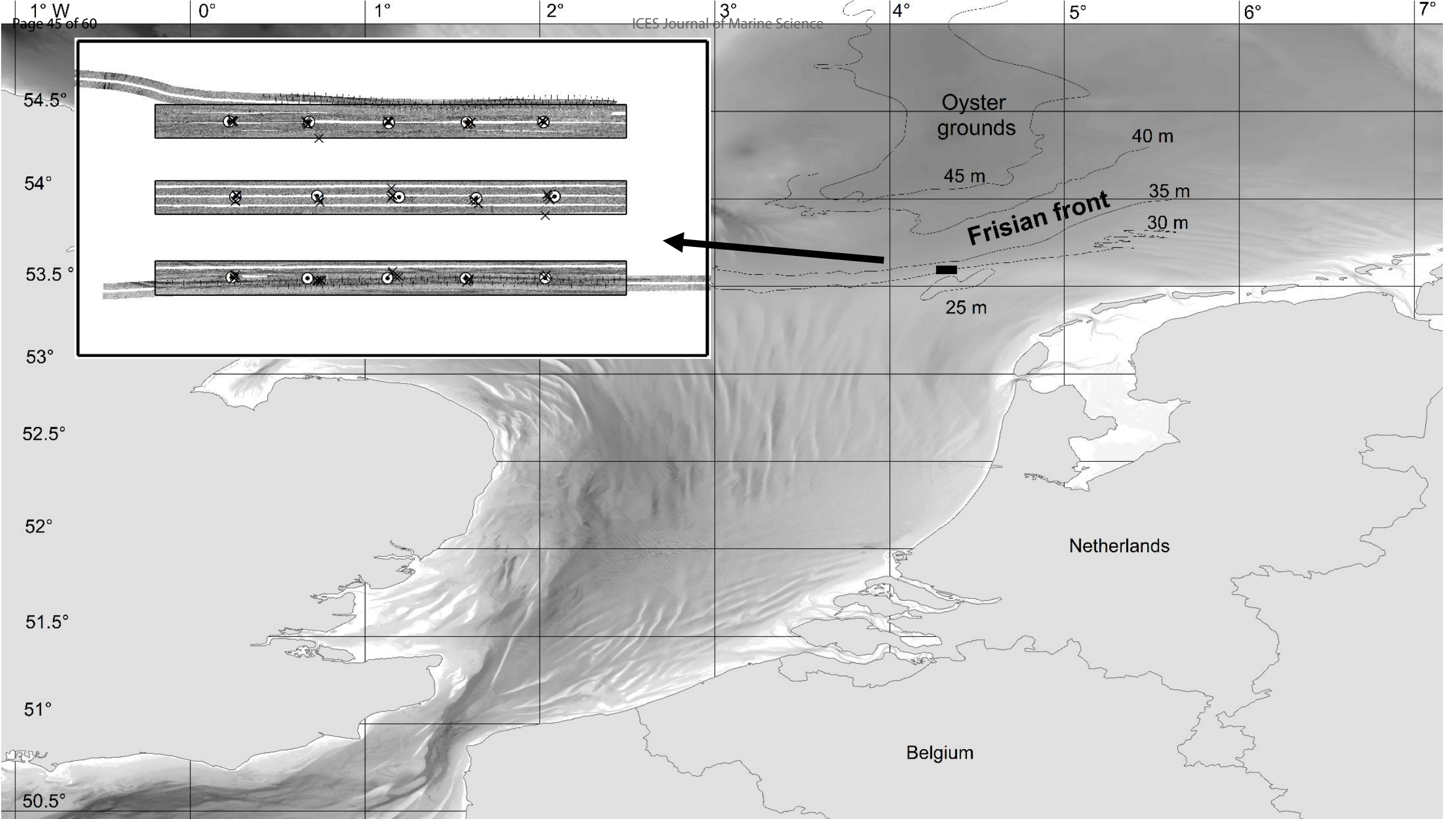
1° W
0°
1°
2°
3°
4°
5°
6°
7°
54.5°
54°
53.5 °
53°
52.5°
52°
51.5°
51°
50.5°
Oyster
grounds
40 m
45 m
35 m
30 m
Frisian front
25 m
Netherlands
Belgium

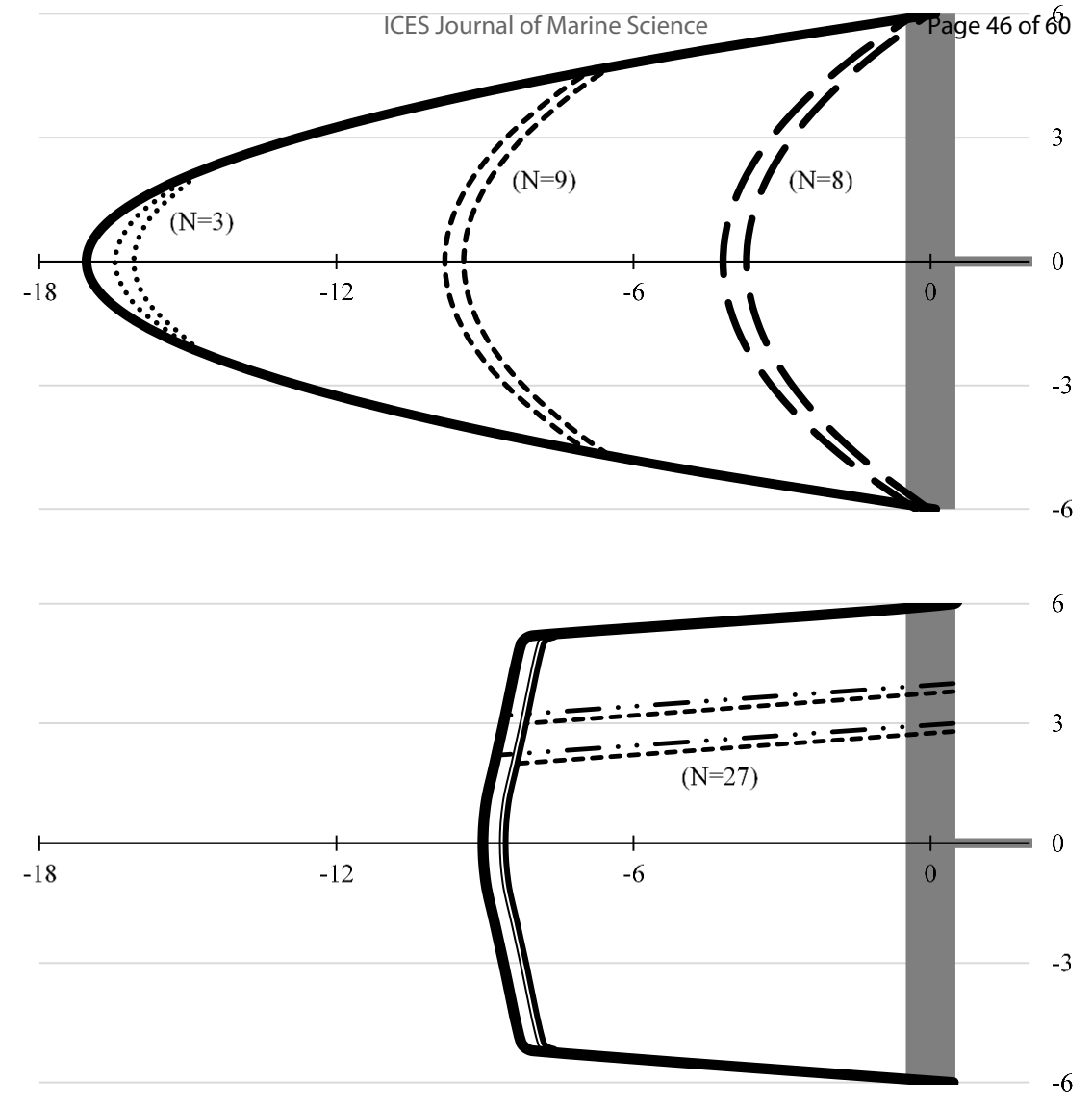
(N=3)
(N=9)
(N=8)
(N=27)
-18
-12
-6
0
6
3
0
-3
-6

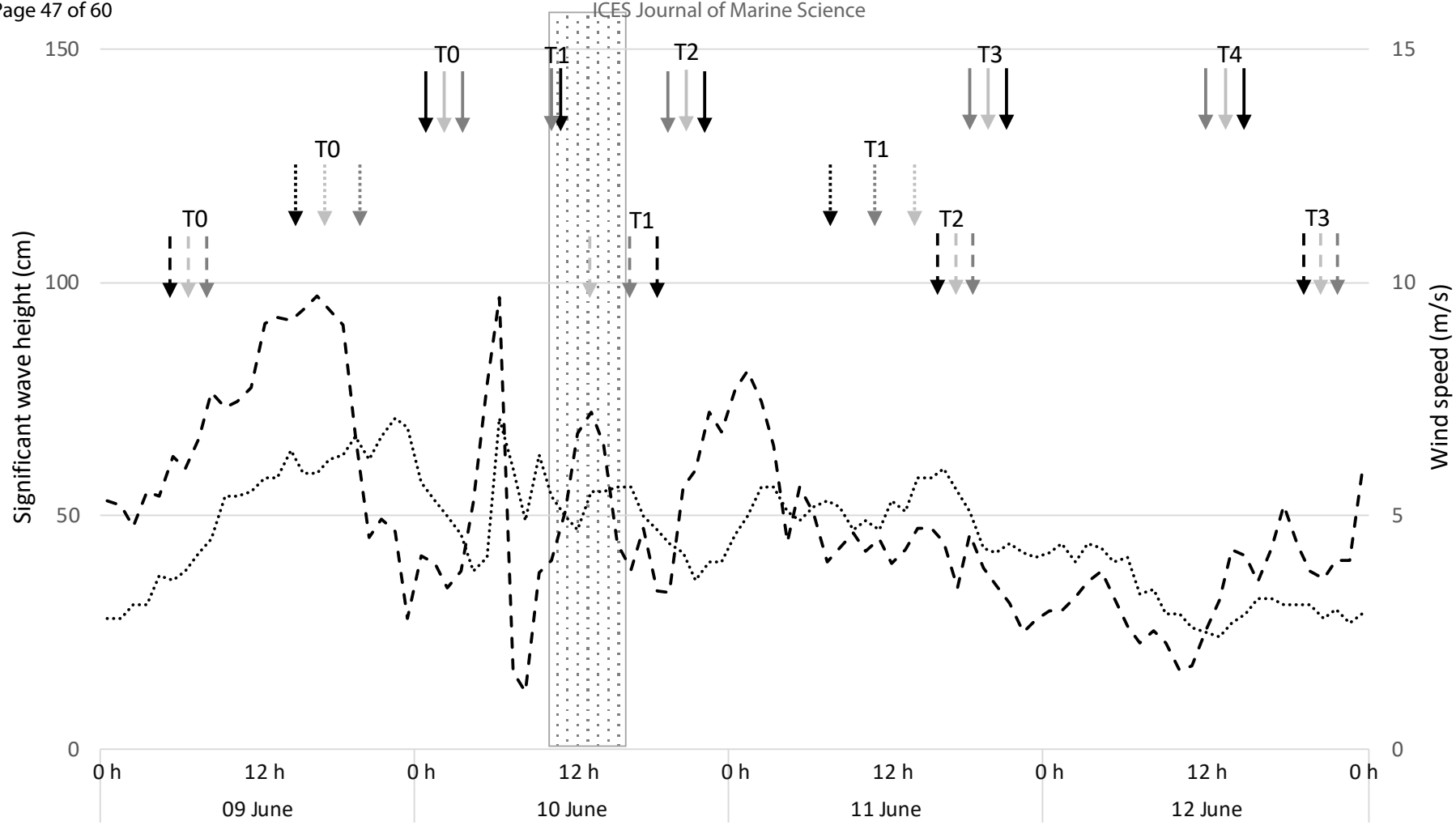
150
100
50
0
15
10
5
0
Significant wave height (cm)
Wind speed (m/s)
T0
T1
T2
T3
T4
0 h
12 h
09 June
10 June
11 June
12 June

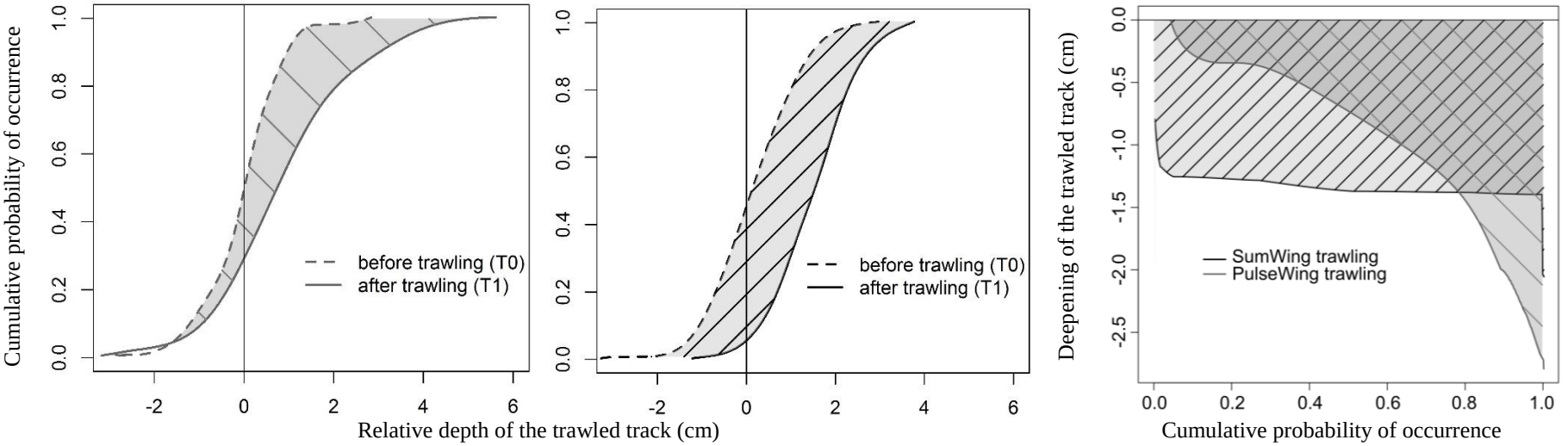
PulseWing trawling
SumWing trawling
Cumulative probability of occurrence
Relative depth of the trawled track (cm)
before trawling (T0)
after trawling (T1)
Deepening of the trawled track (cm)
Cumulative probability of occurrence
SumWing trawling
PulseWing trawling

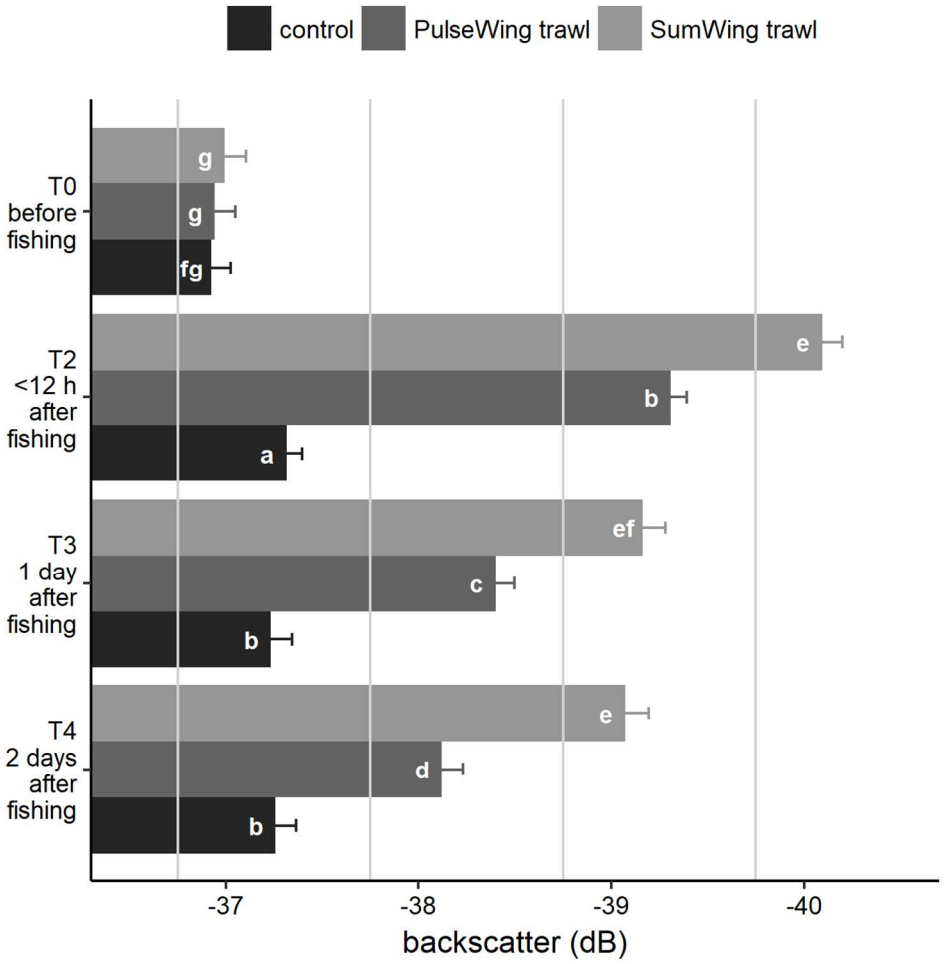

Figure 5 Absorption of sound (acoustic measurement, i.e. backscatter values in dB) of three experimental sites (PulseWing trawl, SumWing trawl and control: no fishing) at various time intervals before and after trawling (Table 1; Figure 3). Letters denote statistical differences ($P < 0.05$) between sites and time intervals.

127x127mm (300 x 300 DPI)

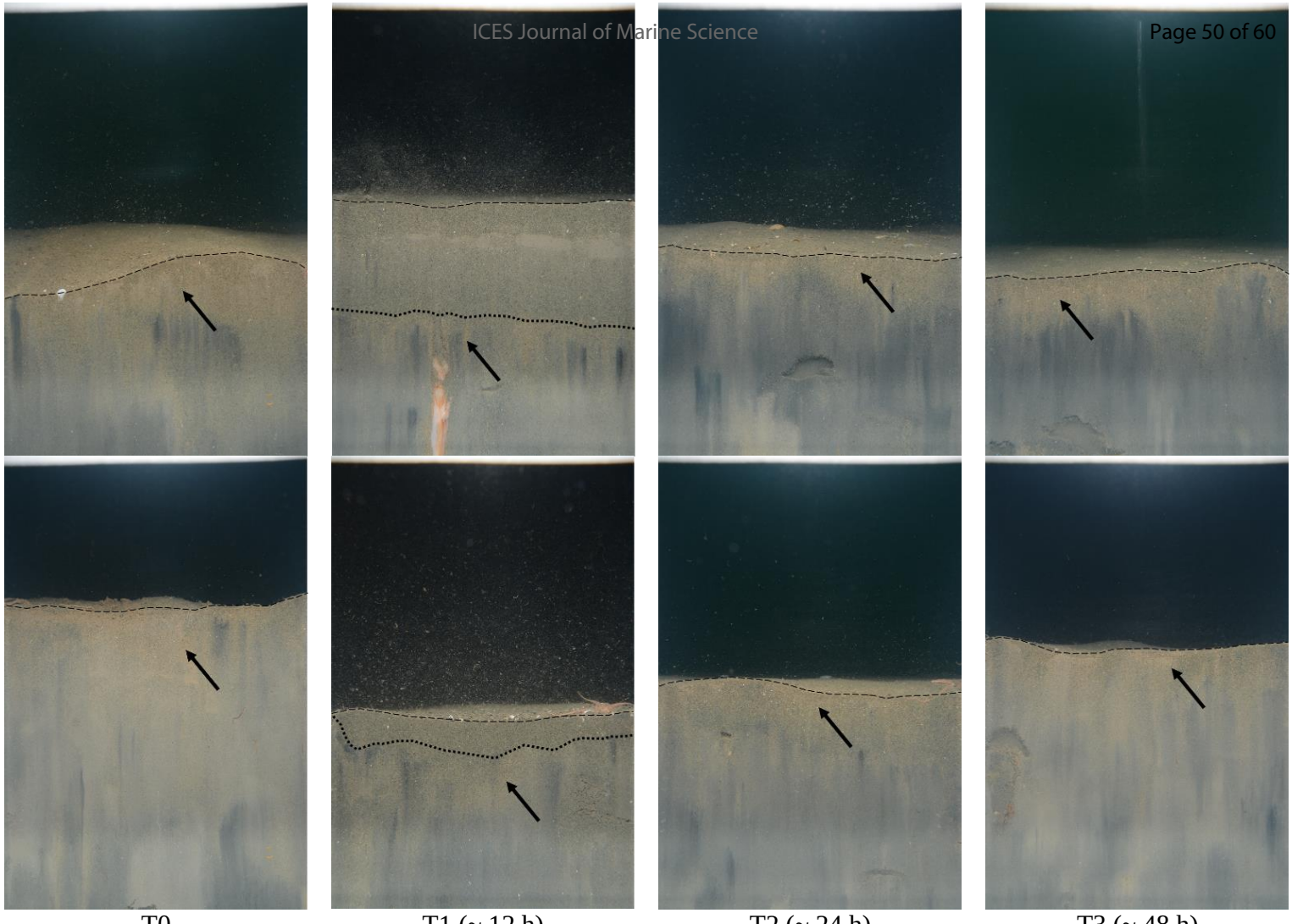
SumWing trawl
PulseWing trawl
T0
T1 (~ 12 h)
T2 (~ 24 h)
T3 (~ 48 h)

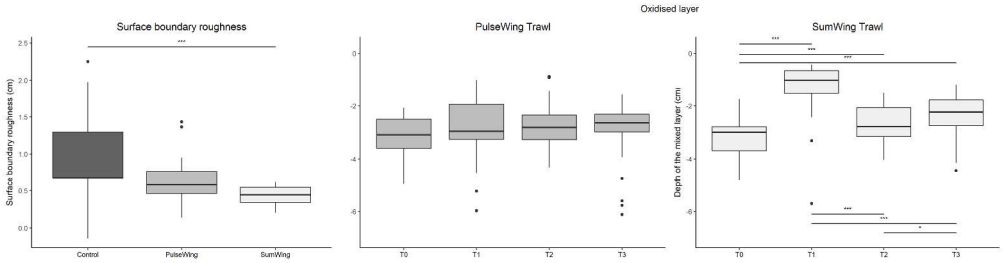

Figure 7 Surface boundary roughness at T1 conditions in the control (dark grey), PulseWing (middle grey) and SumWing (light grey) experimental sites (left panel) and depth of the oxidised layer following PulseWing trawling (middle panel) and SumWing trawling (right panel) at T0, T1, T2 and T3 conditions. Significance levels: * P<0.05; ** P<0.01; *** P<0.001.

465x127mm (300 x 300 DPI)

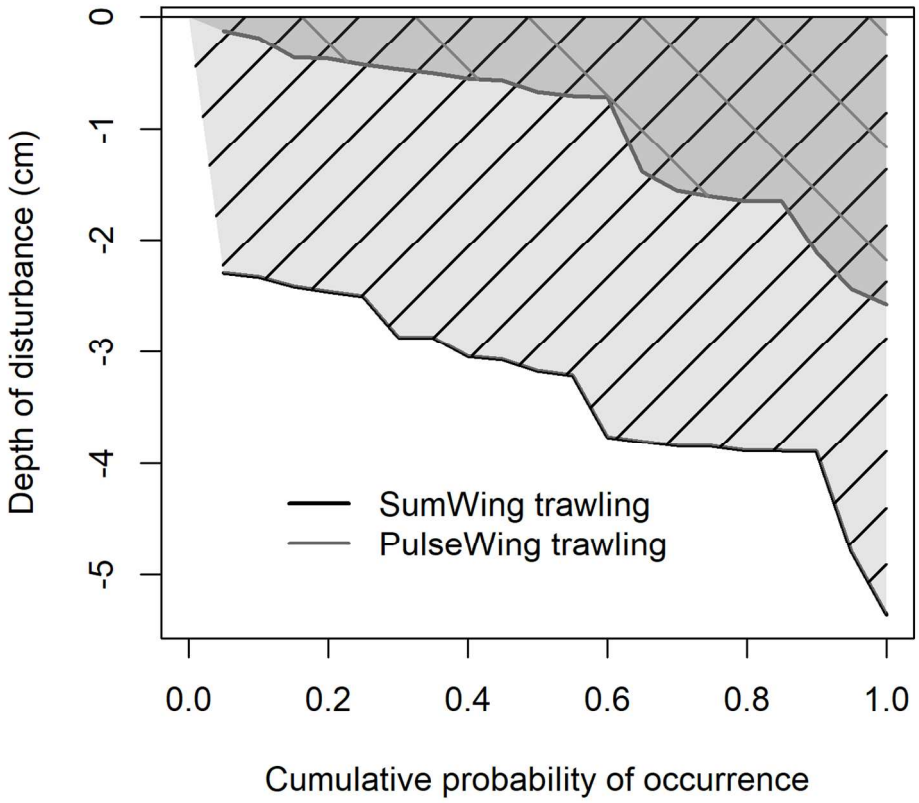

Figure 8 Depth of disturbance following SumWing trawling is deeper than following PulseWing trawling based on the assessment of the SPI images.

127x127mm (300 x 300 DPI)

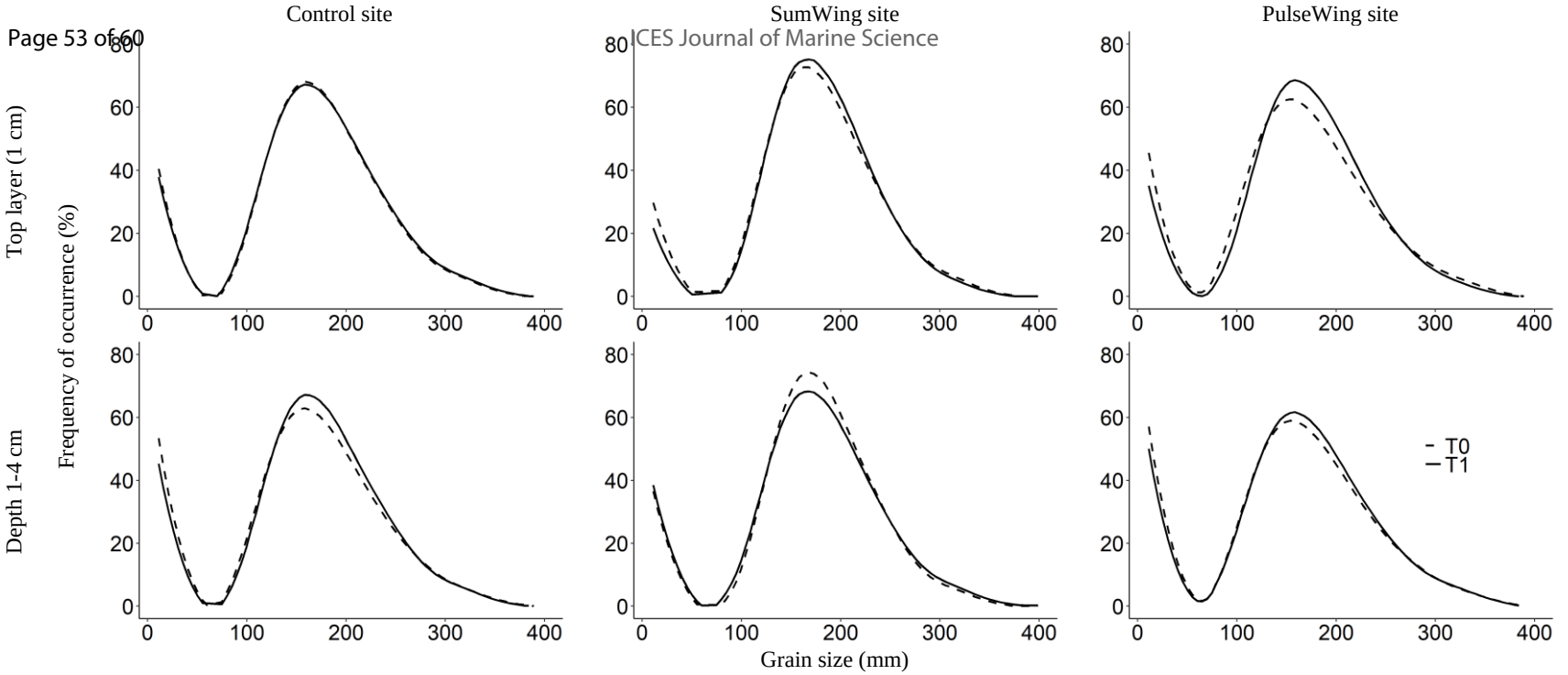
Control site
SumWing site
PulseWing site
Top layer (1 cm)
Depth 1-4 cm
Frequency of occurrence (%)
Grain size (mm)
T0
T1
0
20
40
60
80
0
100
200
300
400

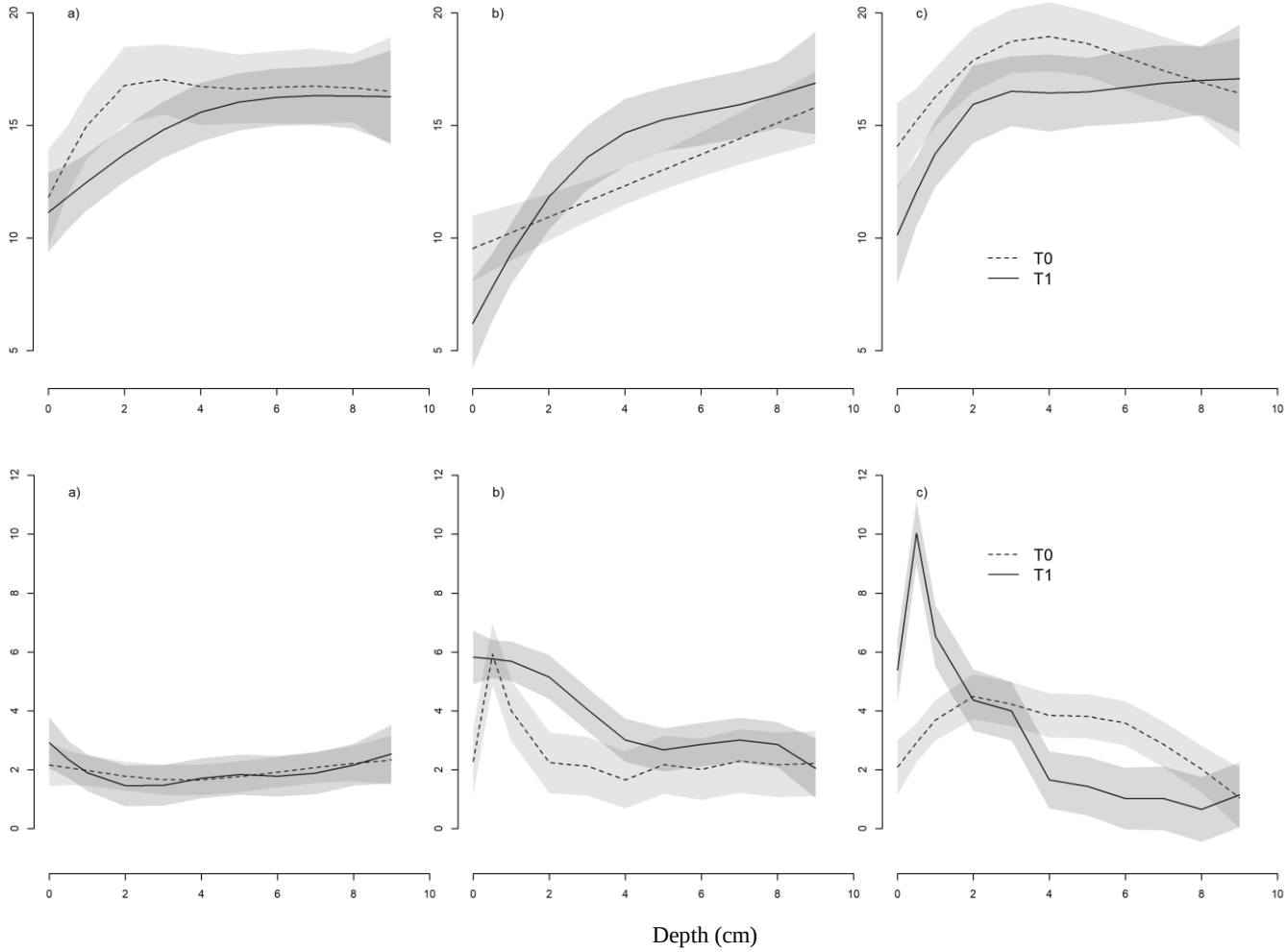
Mean silt fraction (%)
SD of the silt fraction (%)
a)
b)
c)
T0
T1
Depth (cm)

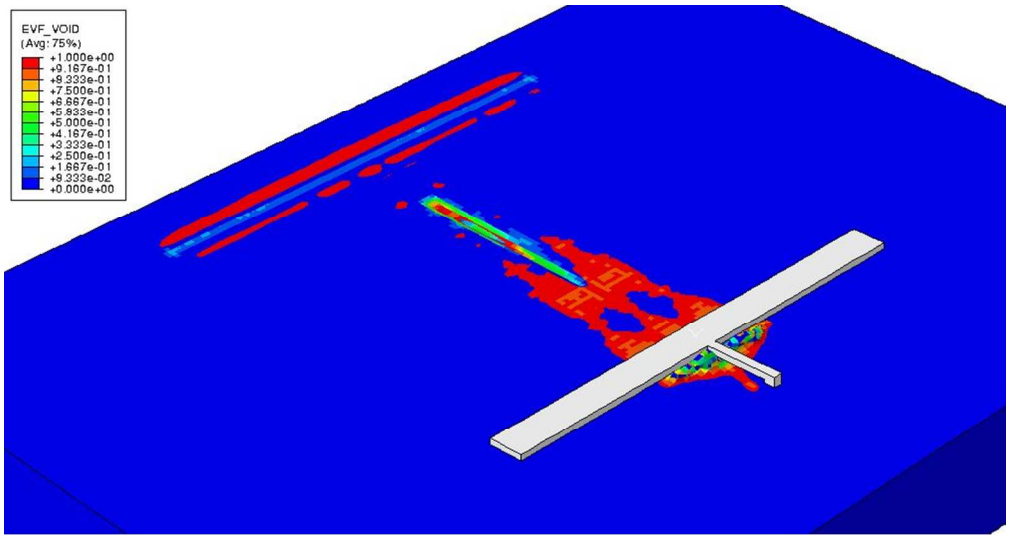

Figure 11 Deformation of the seabed through penetration of the nose of the wing-shaped foil used by the SumWing and the PulseWing trawl. Deformation was measured as the Eulerian Volume Fraction (EVF), which tracks the flow of material through the Eulerian mesh. The value of EVF represents the portion of material filled; EVF=1 indicates that the element is completely filled with the material and EVF= 0 indicates the element is devoid of the material. The wing-shaped foil can move through the Eulerian mesh without any resistance if its volume fraction is zero (blue color).

85x44mm (300 x 300 DPI)

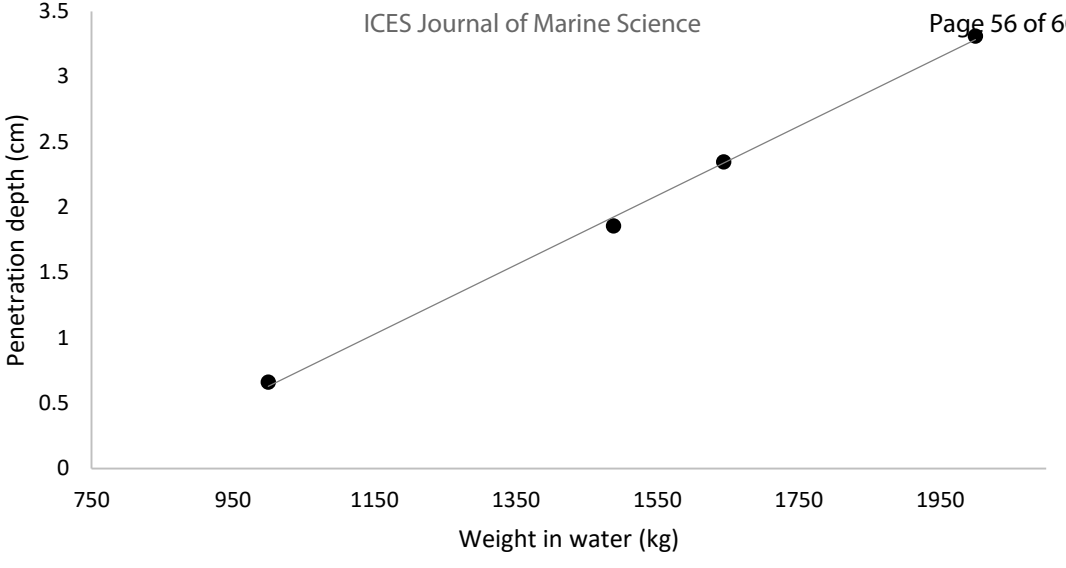
3.5
3
2.5
2
1.5
1
0.5
0
Penetration depth (cm)
750
950
1150
1350
1550
1750
1950
Weight in water (kg)

Table 1 Backscatter values and statistical differences between time intervals (T0, T2, T3, T4) and experimental sites (pulse: PulseWing trawling; control: no fishing; tickler: SumWing trawling). Sites and time intervals with a different letter are statistically different at P-values of 0.05 or $1e^{-6}$. *SD*: standard deviation; CI: 95% confidence interval. Rows are ordered from low to high back scatter values to show which gear and time interval caused the most change in backscatter strength.

Site	Time interval	Description of time intervals	Time lapse (hour)	Backscatter values (dB)				Statistical differences at	
				mean	*SD*	lower CI	upper CI	P < 0.05	P < 1 e^{-6}
tickler	T0	before fishing	-9h48	-36.99	2.34	-37.10	-36.89	fg	d
pulse	T0	before fishing	-7h32	-36.94	2.28	-37.05	-36.84	g	d
control	T0	before fishing	-8h57	-36.92	2.22	-37.02	-36.82	g	d
tickler	T2	< 12 h	5h02	-40.10	2.25	-40.20	-39.99	a	a
pulse	T2	< 12 h	5h02	-39.31	1.87	-39.39	-39.22	b	b
control	T2	< 12 h	5h02	-37.32	1.68	-37.40	-37.24	e	d
tickler	T3	1 d	30h20	-39.16	2.45	-39.28	-39.05	b	b
control	T3	1 d	30h20	-37.23	2.33	-37.34	-37.13	ef	d
pulse	T3	1 d	30h20	-38.40	2.21	-38.50	-38.31	c	c
tickler	T4	2 d	46h36	-39.07	2.54	-39.19	-38.96	b	b
pulse	T4	2 d	46h36	-38.12	2.34	-38.23	-38.01	d	c
control	T4	2 d	46h36	-37.26	2.36	-37.36	-37.15	e	d

Table 2 Track depth (mm) before and after SumWing (tickler) and PulseWing (pulse) trawling. Negative values indicate the deepening of the trawl track.χ^2-values compare water depths inside and outside the trawled track.

Site	Time interval	mean (*SD*)	min	Q1	med	Q3	Max	χ^2(df=1)	*p*-value
tickler	T0	-1.6 (1.0)	32.7	5.2	-1.5	-8.5	-29.7	3.6	0.05791
tickler	T1	-15.1 (0.9)	-9.3	-8.6	-15.2	-20.9	-37.5	93.63	p<0.0001
pulse	T0	0.2 (0.9)	31.9	5.3	-0.2	-5.3	-28.2	0.08	0.77584
pulse	T1	-9.1 (1.6)	28.1	0.5	-7.7	-17.9	-59.5	17.61	p<0.0001

T0, before fishing; T1, immediately following fishing; sd, standard deviation; min, minimum; Q1, first quartile; med, median; Q3, third quartile; max, maximum

Table 3 Estimates of the hydrodynamic drag ($N.m^{-1}$) and sediment mobilisation ($kg.m^{-2}$) from the netting panels, the ground gear assemblies, the noses of the wing-shaped foil and the total gear assemblage of a SumWing and PulseWing trawl.

	Towing speed (kn)	Silt (%)	Netting	Ground gear assemblage	Noses	Total	
Hydrodynamic drag per metre swept ($N\,m^{-1}$)							
SumWing trawl	6	-	1995	1986	84	3817	
PulseWing trawl	5	-	3021	722	59	3802	
Mass of sediment mobilised per m^2 swept ($kg\,m^{-2}$)							**Sediment layer (mm)**
SumWing trawl	6	9.3	5.1	5.1	0.4	10.6	6.6
PulseWing trawl	5	14.7	9.9	2.7	0.6	13.1	8.2

Table 4 Comparison of penetration depth of the nose of the wing-shaped foil, tickler chains and electrodes, and estimates of the deepening of seabed bathymetry, the depth of disturbance from SPI images, the depth of sediment reworking (particle size analysis) and the mobilised sediment layer following SumWing trawling and PulseWing trawling. The total penetration depth was based on the sum of the depth of disturbance and the mobilised sediment layer. All measurements are in cm. Estimates of MBES and SPI measurements and calculations of the total penetration depth are reported as the mean and their standard deviations between brackets.

Parameter of seabed impact	Assessment technique	SumWing trawl	PulseWing trawl
Deepening of seabed bathymetry	MBES[1]	1.5 (0.9)	0.9 (1.6)
Depth of disturbance	SPI[2]	3.4 (0.9)	1.0 (0.8)
Depth of sediment reworking	Box corer samples	<4	<2
Penetration depth of the nose of the wing-shaped foil	Numerical model	2.3	1.9
Penetration depth of a single tickler chain or electrode	Numerical model	1.7	1.2
Mobilised sediment layer	Hydrodynamic model	0.7	0.8
Total penetration depth	Summation	4.1 (0.9)	1.8 (0.8)

[1]MBES: multi-beam echo sounder; [2]Sediment Profile Imagery